REVIEW

Regulation of the Degree of Interpenetration in Metal–Organic Frameworks

Gaurav Verma[1] · Sydney Butikofer[1,2] · Sanjay Kumar[3] · Shengqian Ma[1]

Abstract

Interpenetration in metal–organic frameworks (MOFs) can have significant impacts on the structure, porous nature, and functional applications of MOFs. Considered to be disadvantageous in the initial phases leading to a decrease in surface area, interpenetration has proved to be highly useful for modulation of pore size and selective separation of gases. The importance of interpenetration has been realized over the last decade, and numerous approaches to graft interpenetration and utilize it for improved functions and applications have been achieved. Several factors such astemperature, solvent system, time duration and steric aspects of the ligands have been utilized to regulate the degree of interpenetration (DOI). In this review, we summarize recent advances in regulating the DOI in MOFs and its impact on the resulting properties.

Keywords Degree of interpenetration · Metal–organic frameworks (MOFs) · Ligand design · Partial interpenetration

1 Introduction

Metal–organic frameworks (MOFs) are ordered porous crystalline materials built from metal ions/clusters and polytopic organic linkers forming infinite coordination networks [1–6]. Along with their reticular synthesis, topologically diverse

✉ Shengqian Ma
   sqma@usf.edu

1   Department of Chemistry, University of South Florida, 4202 E. Fowler Avenue, Tampa, FL 33620, USA

2   Department of Chemical and Biomolecular Engineering, University of Illinois at Urbana-Champaign, Champaign, IL, USA

3   Department of Chemistry, Multani Mal Modi College, Patiala, Punjab 147001, India

structures, tunable porosities, uniform pore sizes and extraordinarily high surface areas [7–12], they have shown innumerable applications in gas storage and separation, catalysis, sensing, magnetism, biomedical delivery, etc. [13–18]. Over the past two decades, this field has seen tremendous growth, and the number of publications related to synthesis, structure and applications of MOFs rises exponentially every year. Pioneered initially by great synthetic chemists and crystal engineers, the field now encompasses researchers across all fields, ranging from chemistry, physics, material science, mathematics, and biology to engineering [19, 20].

In recent years, the focus has been directed towards understanding the design criteria and the underlying structure–function relationships [20–22]. The principles governing the directed assembly of these frameworks are gaining importance in terms of linker design, synthetic methodology, and particle morphology [20]. Most of the reports in the literature focus towards the applications, with less consideration of the structural aspects and synthetic methodology. However, there has been a growing number of fascinating reports that can link function with the modulation of synthetic approaches, which give rise to interesting phenomena [12, 23–26]. Interpenetration is one such aspect, in that it can affect the size and shapes of the pores within the framework structure. Interpenetration can be described as the phenomenon by which the large void space in the open framework structures can accommodate one, or more than one, additional network. Though there are no chemical bonds between these additional networks, these are mechanically entangled amongst each other and it is not possible to separate them without the breakage of the bonds [27–32]. The aim in the early stages was to get materials with as high surface areas as possible. So, interpenetration was considered disadvantageous due to reduced surface areas and pore volumes. But now its importance has been realized, and it has come to the fore, establishing greater stability and rigidity as well as enhanced separation capabilities in the frameworks [27, 31–36].

The presence of a large solvent-accessible void in a single network prompts the dual nets catenated with each other to have as minimum void space as possible, leading to interpenetration [37, 38]. However, interpenetration does not necessarily prevent the possibility of obtaining MOF materials having large surface areas. The interpenetrated nets are mechanically entangled with one another, and a single network cannot be separated without the breakage of bonds. Interpenetration enhances the stability of the framework by close interactions such as supramolecular interactions, including hydrogen bonding, π–π stacking and van der Waals forces. Often, interpenetration endows the interpenetrated MOFs with structural flexibility. The interactions between the pore surface and guest molecules can be significantly enhanced by interpenetration [31, 34, 39–42]. Interpenetration can assist CO_2 uptake, increasing the isosteric heat of adsorption [43, 44]. The enhanced CO_2 adsorption can arise from the stepwise filling of pores and framework flexibility. Interpenetration in MOFs can also enhance the separation of gases and storage. Structural interpenetration plays an important role in the functional improvement of MOFs [34, 44–47].

A number of interpenetrated MOFs have been reported, and in-depth reviews highlighting their importance and control over interpenetration have appeared in the literature [27, 28, 31–36, 41, 48–50]. However, the factors used to regulate

interpenetration still need more generalization, and emphasis needs to be given to understanding the factors governing the formation of interpenetrated networks and their modulation. In this review, we aim to highlight recent developments in the constructions of interpenetrated MOFs, and regulation of the degree of interpenetration (DOI) in these networks via change in temperature, modulation of solvent system, time duration and ligand design. We also describe briefly the effects of different degrees of interpenetration on some functional applications (Scheme 1).

2 Importance of Interpenetration in MOFs and Its Applications

The regulation of DOI is important as, in some cases, the non-interpenetrated forms show high surface area and better porosity, whereas in others, a higher DOI might be needed for better separation and enhanced capability due to the high density of the framework.

The number of publications relating to interpenetration has seen a gradual rise over the past two decades, and more publications are being added to the literature every year (Fig. 1). Although interpenetration is often seen as an undesirable result due to the decrease in pore volume, tunability of interpenetration has several important applications in MOF design. Interpenetration often results in MOFs with greater structural and chemical stability. A weakness for most porous MOFs is the
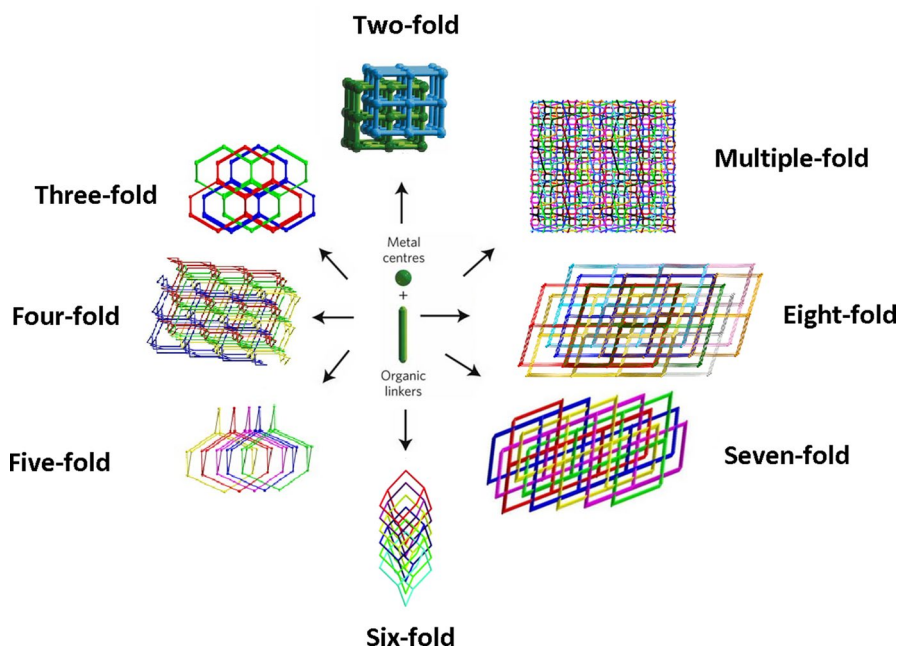
Scheme 1 Depiction of the degree of interpenetration (DOI) in metal–organic frameworks (MOFs) varying from twofold, threefold, fourfold, fivefold, sixfold, sevenfold, eightfold, up to multiple-fold. Adapted with permission from Refs. [81, 86, 88, 126, 127, 131, 132]
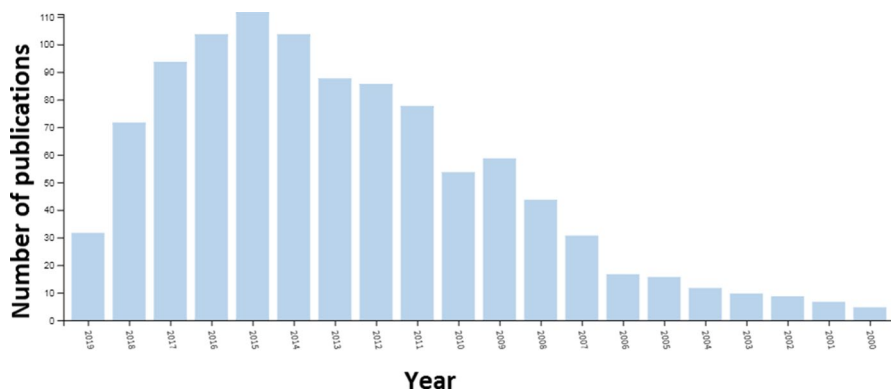
Fig. 1 Growth in the number of publications on interpenetration over the past two decades [135]. Adapted from Web of Science search on frameworks reported with the terms "metal–organic frameworks" and "interpenetration" in all databases from 2000 to 2019

tendency to collapse into nonporous frameworks due to the removal process of the guest molecules. Interpenetrated frameworks have been proven to effectively preserve the pores and avoid this structural collapse [26–29, 44].

## 2.1 Effect of Interpenetration on Pore Environment, Size and Stability

Interpenetration reduces the available void space, which in turn can create confined narrow pores/channels that can be used to trap the guest in the strong electrostatic potential well. The reduced pore size leads to better separation capabilities.

Babarao et al. [51] investigated the effect of pore functionalization on the interpenetrated topologically equivalent IRMOF-9 series. Pore functionalization generally enhances CO_2 uptake for the non-interpenetrated frameworks. However, the authors observed a decrease in CO_2 uptake compared to the non-functionalized IRMOF-9. The smaller pore size seems to play a more important role in CO_2 adsorption. The functionalization enhances the inter-framework interactions, which in turn blocks the small pores that are essential for enhanced CO_2 uptake at low partial pressures (Fig. 2). Thus, Babarao and colleageus concluded that use of small pores in interpenetrated frameworks with a linker having no functionalized groups would be a better choice for enhancing CO_2 uptake at low pressures [51].

In one example, the twofold interpenetrated **MIL-126(Fe)** exhibits higher rigidity than its non-interpenetrated counterpart, **MIL-88** (Fig. 3), resulting in its application as a heterogeneous catalyst. **MIL-88** is not viable for this application as it collapses to a closed pore and forms a nonporous material. Via interpenetration, **MIL-126** maintains high porosity and contains a large number of accessible Lewis acid sites [52–56].

Interpenetration also has unique effects on gas uptake. Ma et al. [47] studied the role of interpenetration in hydrogen uptake in **PCN-6** and **PCN-6′** (Fig. 4). The twofold interpenetration of **PCN-6** led to a 133% increase in volumetric hydrogen uptake from **PCN-6′**, its non-interpenetrated counterpart. Interpenetration in this

Fig. 2 Schematic representation of IRMOF-9 (top) and iodo functionalised IRMOF-9 (bottom), with inter-framework distances of 8.3 Å and 6.2 Å, respectively, showing accessible (*yellow spheres*) and inaccessible (*dark green spheres*) small pores for gas uptake. Reproduced with permission from Ref. [51]
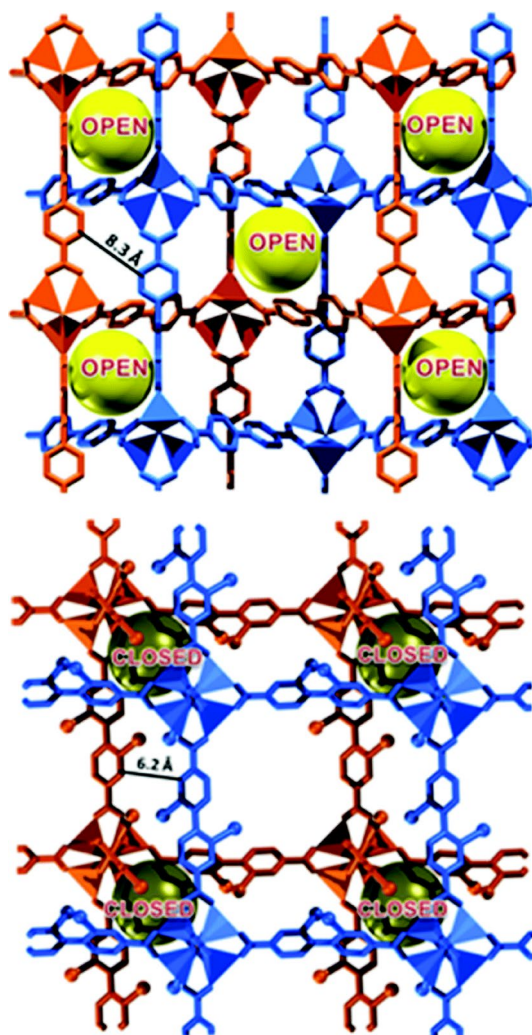
isomer pair also led to a 41% increase in Langmuir surface area. This counterintuitive increase was attributed to the new adsorption sites as well as small pores formed upon catenation that strengthened interactions between gas molecules and the pore walls [47].

Interpenetration in MOFs has also been shown to be effective in gas separations. Gas separations have important applications in the production of clean energy and purification of chemicals. Jiang et al. [57] reported successful separation with **SIFSIX-14-Cu-i**, a twofold interpenetrated copper coordination network. **SIFSIX-14-Cu-i** acts as a molecular sieve, with excellent CO_2 uptake under the ambient conditions, while excluding CH_4. Interpenetration in this
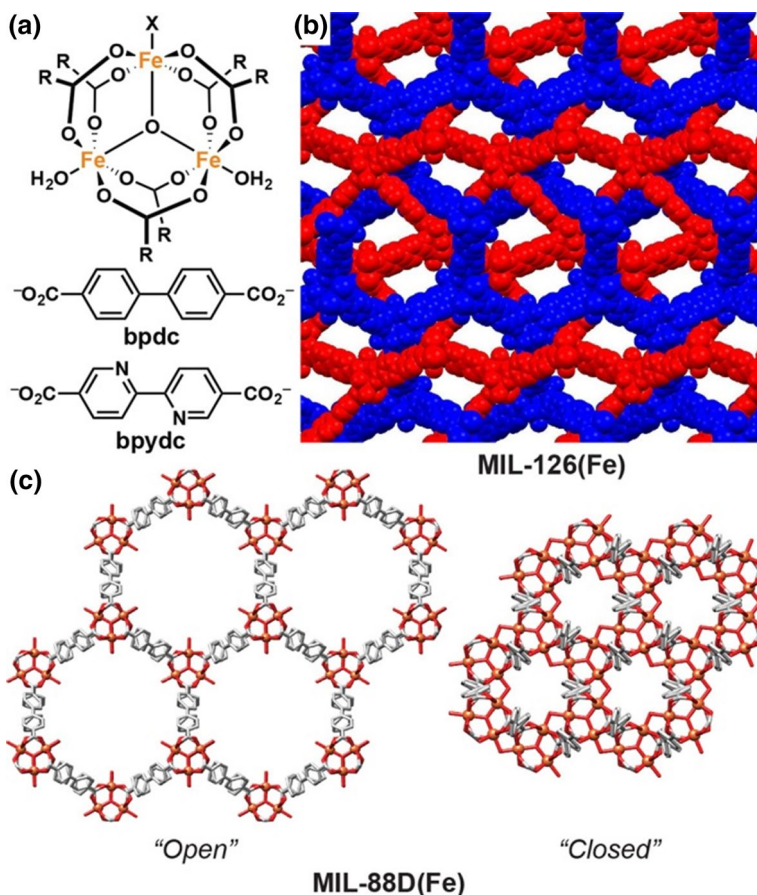
Fig. 3 a Structures of the $[Fe_3O(RCO_2)_6(H_2O)_2X]$ (X = monoanion) secondary building unit (SBU) and linear dicarboxylate linkers. **b** Packing structure of the twofold interpenetrated MIL-126(Fe). **c** Packing structures, viewed down the *c* axis, of open and closed MIL-88D(Fe), generated from simulated structures. Reproduced with permission from Ref. [52]

MOF led to close molecular interactions that facilitated the contraction of pore window size between the kinetic parameters of CO_2 and CH_4 [57].

Lahoz-Martin et al. [58] also observed larger adsorption selectivity in the interpenetrated IRMOFs (IRMOF-9, -11 and -13) compared to their non-interpenetrated counterparts (IRMOF-10, -12 and -14, respectively). In their pore size distributions, IRMOF-9, 11, -13, and -15 showed variety of cavities of 12 Å in dimeter at the maximum. These structures had the perfect combination of pore volume and crannies favoring specific small molecule adsorption. The authors further found that IRMOF-11 and -13 were optimal for ethane/ethylene separation with ethane selectivity [58].
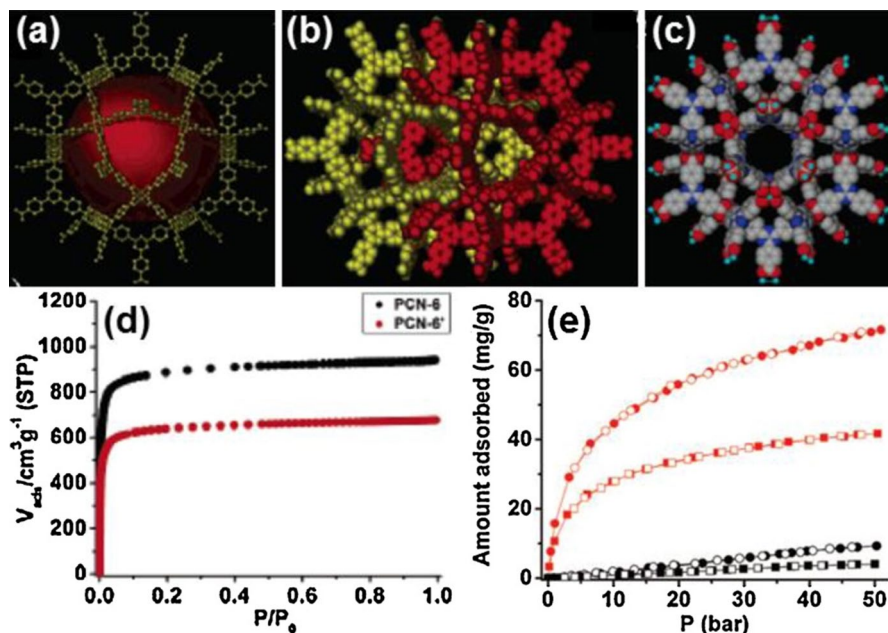
Fig. 4 a Cuboctahedral cage with the inner void highlighted with *large red sphere*. **b** Space-filling model of the interpenetrated nets in PCN-6 and **c** noninterpenetrated net in PCN-6′. **d** N_2 sorption isotherms of PCN-6 and PCN-6′ at 77 K upon activation at 50 °C. **e** Excess hydrogen sorption isotherms of PCN-6 and PCN-6′ at 77 K (*red*) and 298 K (*black*): *circles* PCN-6; *squares* PCN-6′, *solid symbols* adsorption, *open symbols* desorption. Reproduced with permission from Ref. [47]

2.2 Flexibility in MOFs Due to Interpenetration

Certain interpenetrated MOFs also have applications as flexible materials. Yang et al. [59] reported a flexible sixfold interpenetrated MOF, **X-dia-1-Ni-a1**. Despite the high level of interpenetration, it maintains a high void volume of 49%. This MOF undergoes solvent and pressure-induced single-crystal-to-single-crystal (SCSC) transformation to less open phases. Upon heating in vacuo, **X-dia-1-Ni-a1** underwent dramatic structural changes to form a non-porous dia net, **X-dia-1-Ni-c1**, with only 2% solvent-accessible volume. The stability of the c1 form was attributed to interactions between interpenetrated networks (Fig. 5). This MOF exhibits CH_4-induced reversible switching and has applications in natural gas storage [59].

3 Factors Regulating DOI

The DOI has been shown to be tunable based upon different controls during the MOF synthesis. Precise control of interpenetration is imperative due to the benefits and drawbacks associated with the application of interest. Although a high interpenetration in the structure imparts high thermal stability and selective recognition for small molecules on the one hand, it leads to a low free volume on
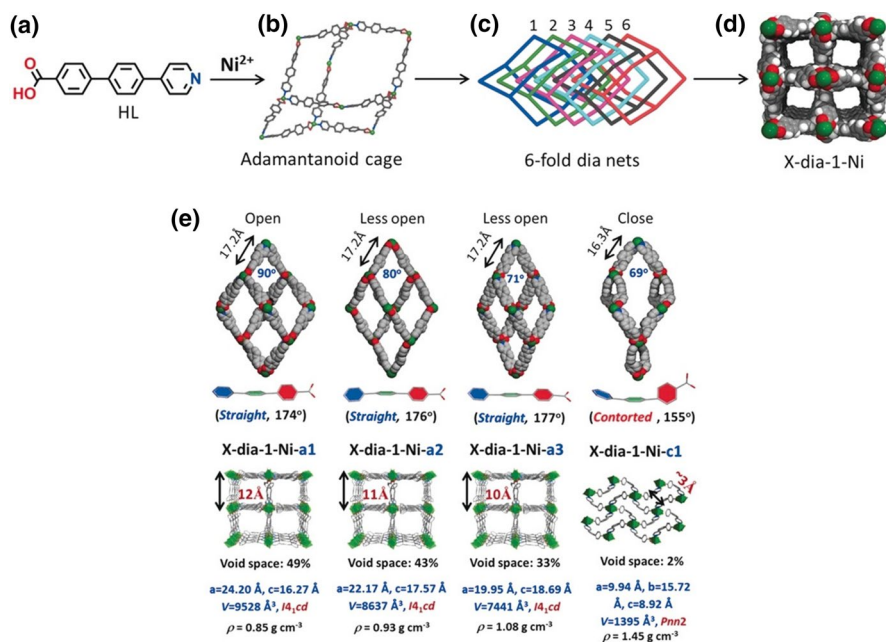
Fig. 5 **a** Structure of 4-(4-pyridyl)-biphenyl-4-carboxylic acid (HL). **b** Adamantanoid cage in NiL$_2$. **c** Sixfold interpenetrated dia nets in NiL$_2$. **d** Rectangular channels viewed along the *c*-axis. **e** Single crystal structures of the porous (a1, a2, a3) and non-porous (c1) phases of X-dia-1-Ni. Reproduced with permission from Ref. [59]

the other, limiting applications for catalysis and macromolecule separation that require a larger free space for diffusion. A lower DOI, or even non-interpenetration, can lead to higher free volumes and surface areas, but there is a trade-off in terms of poor structural stability and an absence of channels for the encapsulation of small guests. A control over the DOI to synthesize the material with the desired porosity and functionality remains challenging due to the interplay of a number of factors, such as temperature, concentration, pH, modulator and ligand design. Furthermore, partial interpenetration in the MOFs can be controlled by such parameters to get a mixture of interpenetrated and non-interpenetrated counterparts. Even the breathing behavior can be tuned through interpenetration, which can be used for modulation and control of some functional properties. Another strategy to control interpenetration is the introduction of solvent molecules with different sizes that can act as the space-filling templates in the pores [27, 28, 34].

Lapidus et al. [60] utilized high pressures to generate porosity and polymorphism in nonporous molecular framework Zn(CN)$_2$. In large molecule fluids or no fluids, the doubly interpenetrated dia framework transforms to orthorhombic polymorph Zn(CN)$_2$-II (*Pbca*) with distortions in the structure. In case of the small molecule fluids, the nonporous interpenetrated Zn(CN)2 framework can undergo reiterative transitions forming porous, non-interpenetrated polymorphs with different
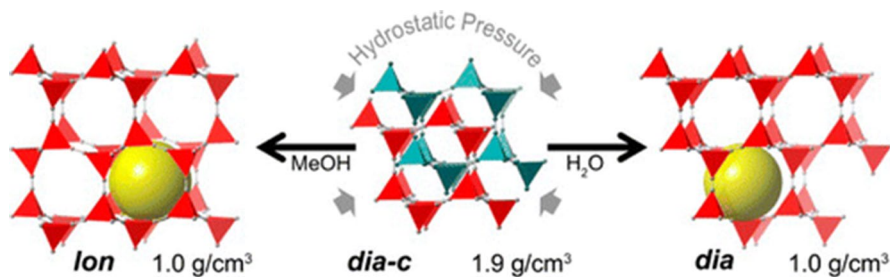
Fig. 6 Formation of different phases under pressure for $Zn(CN)_2$. Reproduced with permission from Ref. [60]
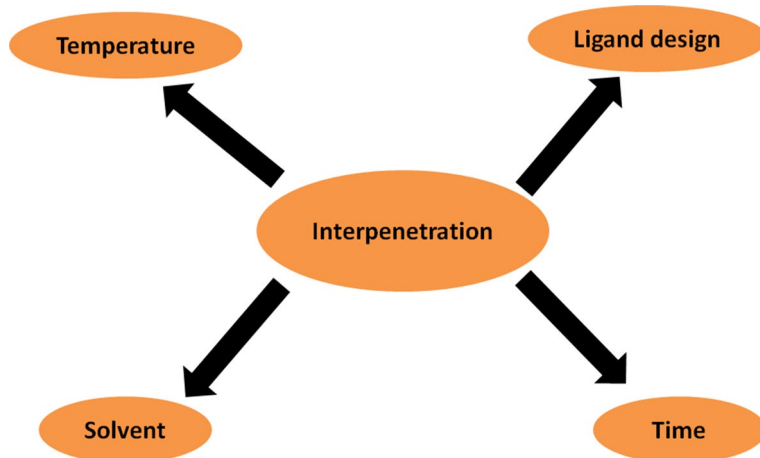

Fig. 7 Factors affecting the DOI in MOFs

topologies (Fig. 6). Space filling of the interpenetrated framework plays an essential role in pressure-induced reconstructive transitions [60].

For the purpose of this review, we will focus on studies relating DOI to variables such as temperature, solvent, time, and ligand design (Fig. 7).

3.1 Temperature

Higher temperature generally has been shown to favor increased DOI. Through increased kinetics, faster crystal growth occurs, increasing the possibility of interpenetrated MOFs. For this reason, higher reagent concentration is also associated with increased interpenetration. One example of this effect has been shown in a study where **[Co$_2$(ndc)$_2$(bpy)]**, a doubly interpenetrated framework (Fig. 8), has been synthesized in its triply interpenetrated isomeric form simply by increasing the crystallization temperature, whereby an intermediate form was also isolated [61].
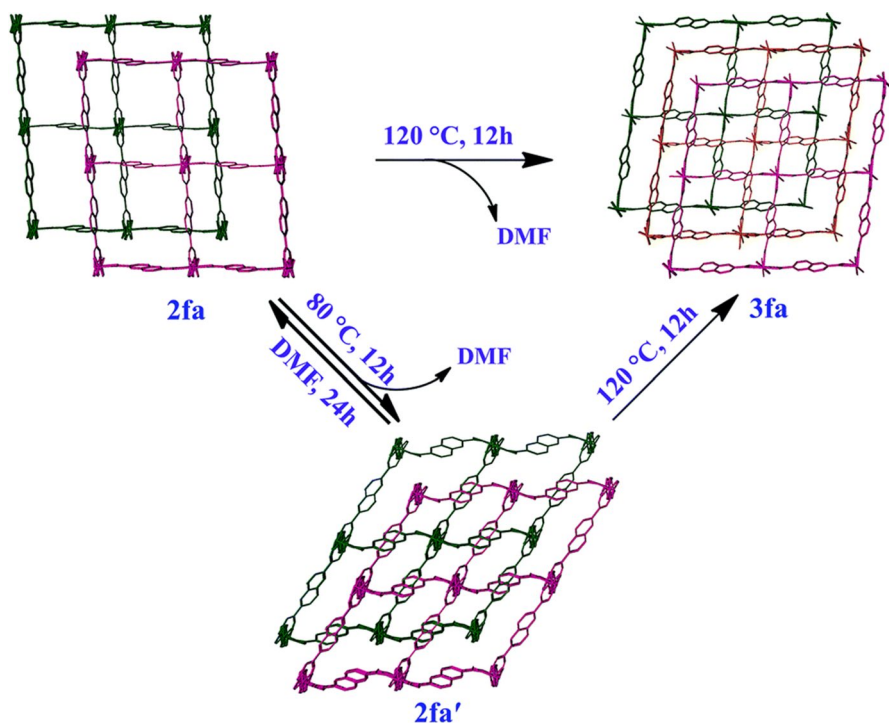
Fig. 8 Representation showing bending and switching of interpenetration in the $[Co_2(ndc)_2(bpy)]$ system. Reproduced with permission from Ref [61]

Zhang et al. [62] further investigated this effect on a non-interpenetrated form of **[Cd(bipy)(bdc)]**, denoted as **1**, and **[Cd(bipy)(bdc)]**, its doubly interpenetrated isomer, denoted as **2** (Fig. 9).

These authors were able to systematically tune the level of interpenetration by controlling the temperature and concentration (Table 1). They confirmed that interpenetrated crystal selectively formed at high temperature and concentration, while low temperature and concentration favored its non-interpenetrated form. This was theorized on the thermodynamic effect of increased temperature to produce more stable, denser products [62].

Wang et al. [63] studied the effects of temperature-of-reaction-induced interpenetration and also observed an increase in the DOI upon increase in temperature. The doubly interpenetrated **[Co(TTPA)(TPA)$_{0.5}$(H$_2$O)$_2$]·DMA·0.5TPA·H$_2$O$_n$** (**1**) upon immersing in water followed by heating at 50 °C for 6 h is converted to a fourfold interpenetrating framework **[Co(TTPA)(TPA)]· H$_2$O$_n$** (**1a**) via SCSC transformation (Fig. 10). The large hexagonal channels of **1a** and the available void space of 79.8 Å^3 allow for interpenetration with each other. The fourfold interpenetrated network **1a** decomposes at a higher temperature compared to **1**, and the authors attribute the role of temperature in regulating interpenetration as follows: at lower temperatures **1** is preferred, whereas, at higher temperatures, a more thermodynamically stable and densely interpenetrated crystalline state **1a** is generated.
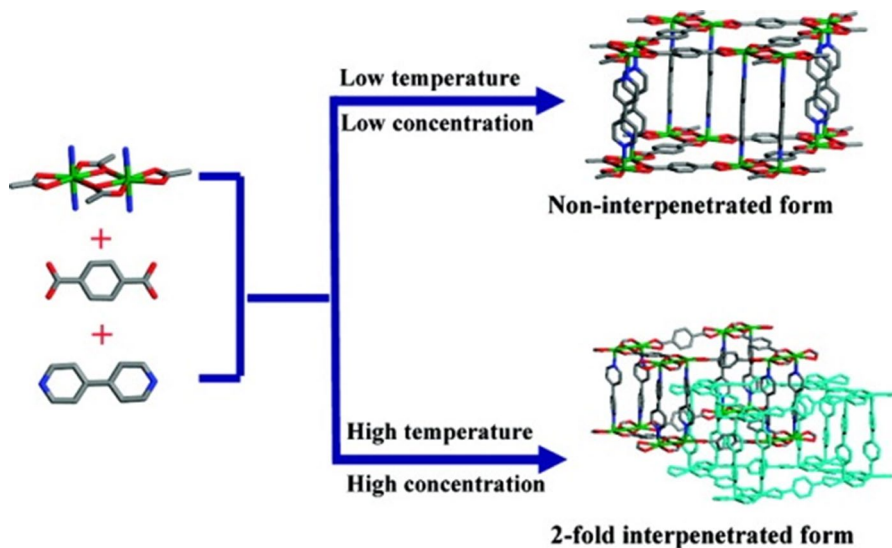
Fig. 9 Control of interpenetrated vs non-interpenetrated form in [Cd(bipy)(bdc)]. Reproduced with permission from Ref. [62]

Table 1 Summary of products isolated at different temperatures and concentrations (?=unknown new phase). Reproduced with permission from Ref. [62]

	0.2M	0.1M	0.05M	0.025M	0.0125 M	0.0062 5M
85°C	?	1	1	1	1	?
95°C	?	1	1	1	1	?
105°C	?	1+2	1+2	1	1	?
115°C	?	2	2	1+2	1	?
125°C	?	2	2	1+2	?	?
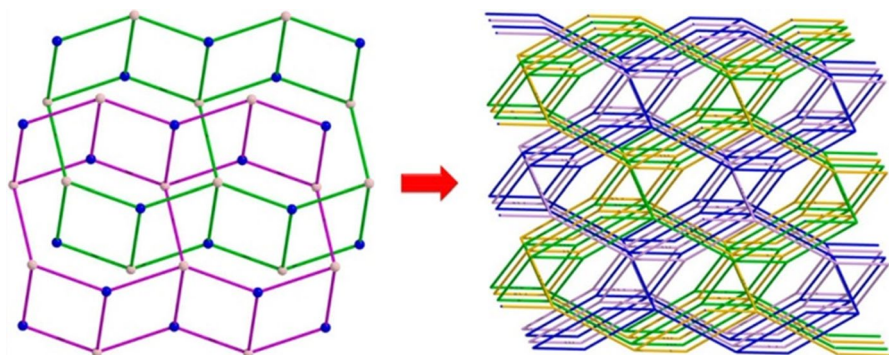
Fig. 10 Single-crystal to single crystal (SCSC) transformation from twofold interpenetrating **1** to four-fold interpenetrating network **1a**. Reproduced with permission from Ref. [63]

3.2 Solvent System

The size of the guest molecules (e.g., solvents, counterions, template molecules) also plays an important role in deciding the fate of interpenetration. The large template molecules mostly lead to lower degree interpenetrated or non-interpenetrated MOFs, whereas the smaller guests give rise to a high DOI.

Elsaidi et al. [64] demonstrated the effect of the crystallization solvent on level of interpenetration in diamondoid nets (Scheme 2). The use of bulkier solvents such as *tert*-butylformamide led to wider channels and a lesser DOI in the synthesized MOFs. This is likely attributable to intermolecular forces and steric hindrances between bulky solvent molecules and forming lattices. This effect is less apparent with respectively less bulky solvents such as ethyl alcohol, reportedly forming smaller channels and higher DOI [64].

Ferguson et al. [65] also extensively tested the effect of solvent on the phenomenon of partial interpenetration (Fig. 11). They theorized that the growth rate of the host-sublattice must exceed that of the interpenetrating sub-lattice to form a partially interpenetrated framework. In bulkier solvents, the interpenetrating sub-lattice is much slower to form, allowing for the collection of partially interpenetrated crystals. Partially interpenetrated forms of **MUF-9** and **MUF-10** were collected from synthesis in a solvent system containing *N,N*-dibutylformamide (DBF) and *N,N*-dimethylformamide (DMF). By adding DMF to DBF, these authors were able to systematically control the degree of partial interpenetration by accelerating the growth of the sub-lattice [65].

Rankine et al. [66] observed that the hydrolysis rate in different solvents plays a critical role in controlling interpenetration for hydroxyl-functionalized IRMOFs (Fig. 12). The reactions in DMF led to faster rate of hydrolysis and interpenetrated framework. They concluded that high molecular weight solvents may be used to control the interpenetration along with steric effects from the ligands [66].
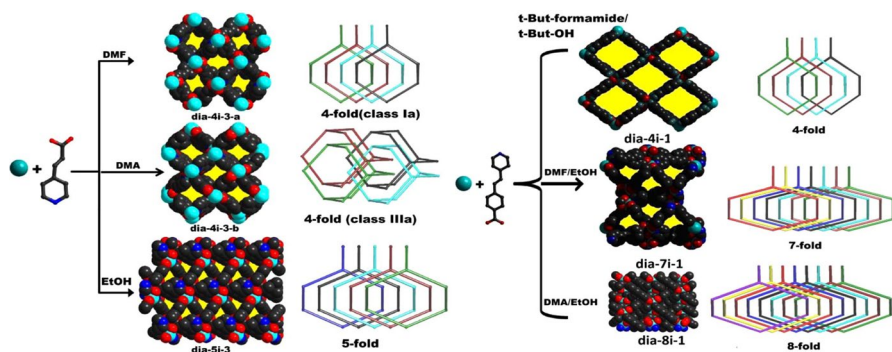
Scheme 2 Schematic representation of the control over the level of Interpenetration in dia nets achieved via solvent templation. Reproduced with permission from Ref. [64]
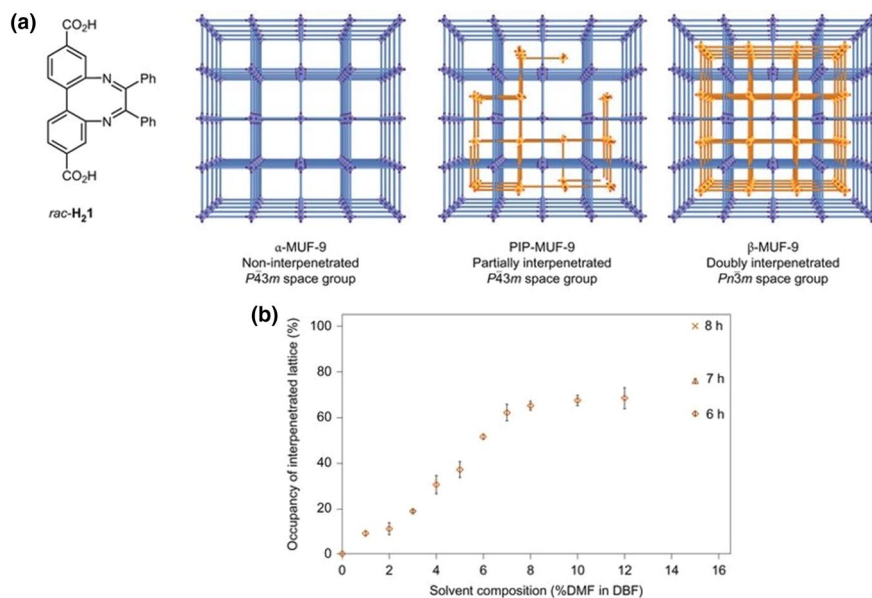
Fig. 11 **a** Nature of the solvent and the reaction time determine whether the combination of *rac*-**H₂1** with $Zn(NO_3)_2$ produces α-MUF-9 (non-interpenetrated), PIP-MUF-9 (partially interpenetrated) or β-MUF-9 (doubly interpenetrated). **b** Composition of the reaction solvent controls the degree of partial interpenetration in MUF-9. Reproduced with permission from Ref. [65]
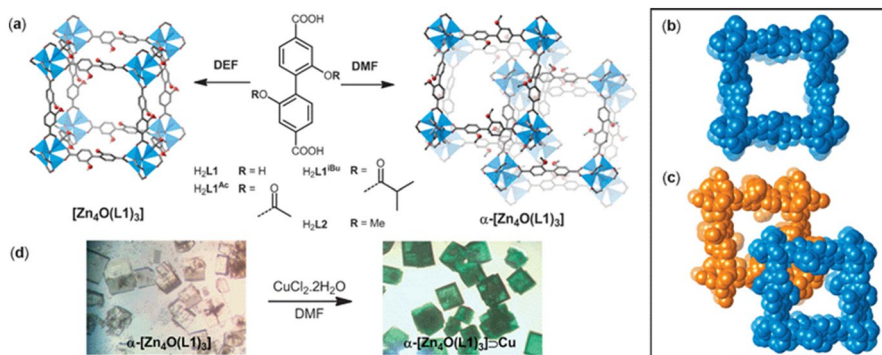
Fig. 12 **a** Synthesis of $[Zn_4O(L1)_3]$ and α-$[Zn_4O(L1)_3]$. *Inset* Space-filling representations of the pores in **b** $[Zn_4O(L1)_3]$ and **c** α-$[Zn_4O(L2)_3]$. **d** Images from the metallation studies to generate α-$[Zn_4O(L1)_3] \supset Cu$ and show accessibility of the hydroxyl groups. Reproduced with permission from Ref. [66]

3.3 Time

The reaction time of the MOF synthesis can have drastic effects on interpenetration. Decreasing the time of a synthesis reaction is associated with enlarged pores and, therefore, decreased interpenetration. Decreased reaction time directly limits the

probability of an interpenetrated net forming. Also, as interpenetrated nets lower the energy of the system by limiting the number of open bonding sites, interpenetration is thermodynamically favorable. Therefore, given enough time, a framework will form the most energetically stable configuration. Ferguson et al. [65] verified this theory with **MUF-9** and **MUF-10**. After an 8-h synthesis in DMF, they determined a 52% partially interpenetrated isomer of **MUF-9**. Upon extending the reaction time, the full twofold interpenetrated isomer, **β-MUF-9**, formed. These authors identified the same phenomenon with **MUF-10**, the enantiopure analogue of **MUF-9**.

3.4 Ligand Design

The design of the ligand affects the DOI based on the following attributes:

- sterically bulky groups on ligand
- elongated linkers

Altering the design of an organic ligand can achieve different levels of interpenetration. For example, the syntheses of **SNU-70** (non-interpenetrated) and **SNU-71** (twofold interpenetrated) differ by the existence of a double bond in the ligand of **SNU-70** (Fig. 13). This slight difference in organic ligand structure leads to interpenetration and vast differences in pore size and gas uptake [67].

Similar to the template effect, the presence of sterically bulky groups on the organic ligand could help prohibit framework interpenetration. However, if the groups on the ligands start to show interaction with each other, it can enhance the possibility of interpenetration if the interacting groups can come closer to each other. Therefore, the goal could be achieved by selective modification of a ligand with pendant groups. Therefore, the use of elongated organic linkers in attempts to synthesize MOFs with expected large pores is generally a very challenging task, as the formation of interpenetrated frameworks may be preferred to increase the stability of the framework. MOFs constructed with longer ligands generally have larger voids, which make them unstable. Thus, interpenetration reasonably occurs to reduce pore space in order to meet the systematic stability requirement in MOFs.
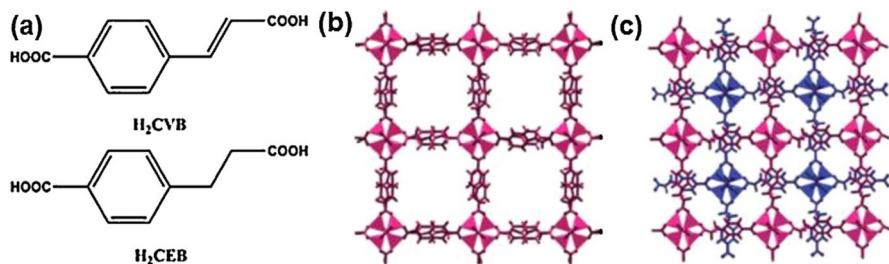
Fig. 13 **a** Ligands used for the MOF synthesis and crystal structures of **b** noninterpenetrated and **c** twofold interpenetrated MOFs. The interpenetrated networks are represented in *red* and *blue* in **c**. Reproduced with permission from Ref. [67]

The use of bulky protecting groups followed by deprotection upon framework formation is another strategy for suppressing the framework interpenetration. Lun et al. [68] utilized bulky thermolabile tert-butoxycarbonyl (Boc) for a proline moiety and its postsynthetic removal produced open MOF with increased pore volume (Fig. 14). Thus, the use of the bulky protective group can preclude framework interpenetration and is an effective strategy to generate open frameworks.

Similarly, the length of the organic ligand has been shown to correlate with the level of interpenetration. Typically, increased length of ligands is associated with a higher probability for interpenetration in a given framework. For example, **PCN-240**, **PCN-245**, and **PCN-248** exhibit increasing degrees of interpenetration, varying only by increasing lengths of the organic ligand (Fig. 15).

The authors observed that the twofold and threefold interpenetration of **PCN-245** and **PCN-248** led to increased framework stability, rigidity, and permanent porosity. Also, **PCN-280** (interpenetrated) and **PCN-285** (noninterpenetrated) were synthesized using mixed ligands of different lengths [69]. This effect of interpenetration control can once again be shown in "Porous Interpenetrated Zr-Organic Frameworks" (PIZOFs). Eight ligands of differing lengths built from a combination of phenylene (P) and ethynylene (E) regulated interpenetration in UiO-type MOFs and PIZOFs (Fig. 16). By decreasing the ligand length from 17 to 15 Å, the product is identified as a non-interpenetrated Zr-MOF of the UiO type instead of a twofold interpenetrated PIZOF. The PEPP linker formed an interpenetrated structure, while the next shortest linker, PEEP, did not allow for interpenetration to occur. The authors noted the increased thermal stability of the PIZOFs, stability in water, and also stability during drying from the water-wetted state [70].

Vincent-Morales and co-workers studied the impact on the flexibility for interpenetrated **MUV-2-i(pyridine)** $(TTFTB)_3[(Fe_3O)(py)_3]_2 \cdot 0.36py$, which shows a
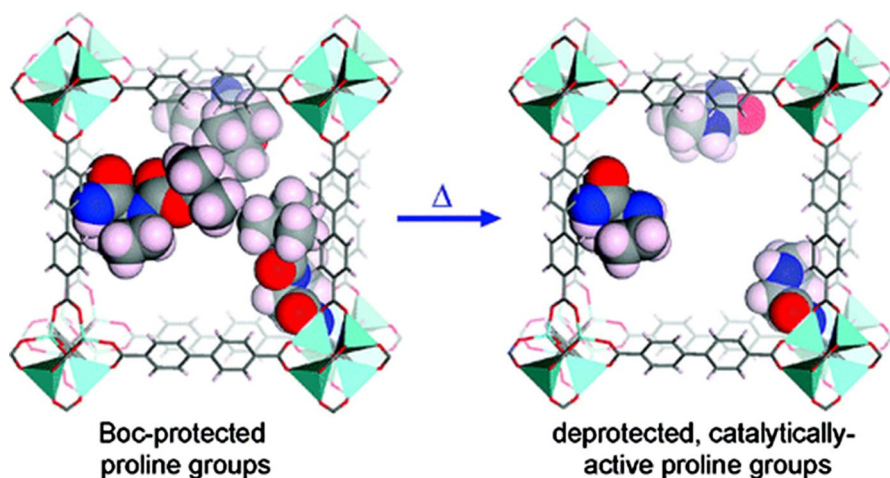
Fig. 14 Schematic of the protection-deprotection strategy using bulky Boc-ligand for transformation of IRMOF-Pro-Boc to IRMOF-Pro suppressing interpenetration. Reproduced with permission from Ref. [68]

remarkable decrease in free volume compared to its non-interpenetrated counterpart **MUV-2** (Fig. 17). Quite interestingly, **MUV-2-i** demonstrates more rigidity upon soaking in polar solvents such as pyridine or DMF compared to **MUV-2**, which shows breathing behavior upon immersing in these solvents. The ligand TFTB molecules in **MUV-2-i** get distorted due to the strain due to the distortion between the two dithiole rings leading to the interpenetrated network with enhanced rigidity and stability in the framework [53].

4 Examples of DOI

MOFs with many different DOIs have been reported to this date. The twofold interpenetration in MOFs is the simplest form of entanglement whereby the parent net accommodates one dual net that can be related by either translation, symmetry operation or both. As the DOI increases, the stability and selectivity is enhanced but it could also lead to a reduction in pore size and the framework could become nonporous. Many interesting features have been observed in case of MOFs with varied DOI. Aesthetically pleasing structures have been generated and many applications have been demonstrated. Here, we focus on some of the fascinating and interesting examples of MOFs with twofold [71–75], threefold [76–81], fourfold [82–86], fivefold [87–90], sixfold [91–96], sevenfold [97, 98], eightfold [99–104] and more than eightfold [105, 106] with a section on the recent phenomenon of partial interpenetration. The terms coordination polymers and MOFs have been used interchangeably in the literature, causing confusion. So, we have tried to keep our focus on examples related to MOFs or porous coordination polymers. Table 2 summarizes some of the classical MOFs with interpenetrated structures.

4.1 Twofold

Liu et al. [114] synthesized two In(III) based MOFs: **FJU-16** and **FJU-17**. **FJU-16** was reported to be fourfold interpenetrated and **FJU-17** was reported to be twofold interpenetrated (Fig. 18). While they have the same single net structure, **FJU-17** exhibits a greater solvent accessible void. **FJU-17** also has a much higher intrinsic proton conductivity than its fourfold interpenetrated counterpart. This was attributed to the higher number of guest molecules in **FJU-17** and available void space. **FJU-17** has potential applications in fuel cells (FCs) as they contain proton conducting materials to promote safe and efficient operation [114].

Gupta et al. [115] reported a doubly interpenetrated water stable MOF $[Co_2(4,4'\text{-bpy})(L)] \cdot H_2O \cdot 0.5(DMF)$ whereby $H_4L = 4,4',4'',4'''$-silanetetrayltetrabenzoic acid and $4,4'$-bpy $= 4,4'$-bipyridine. The authors attributed the stability in water to the presence of interpenetration in the framework and *N*-coordination
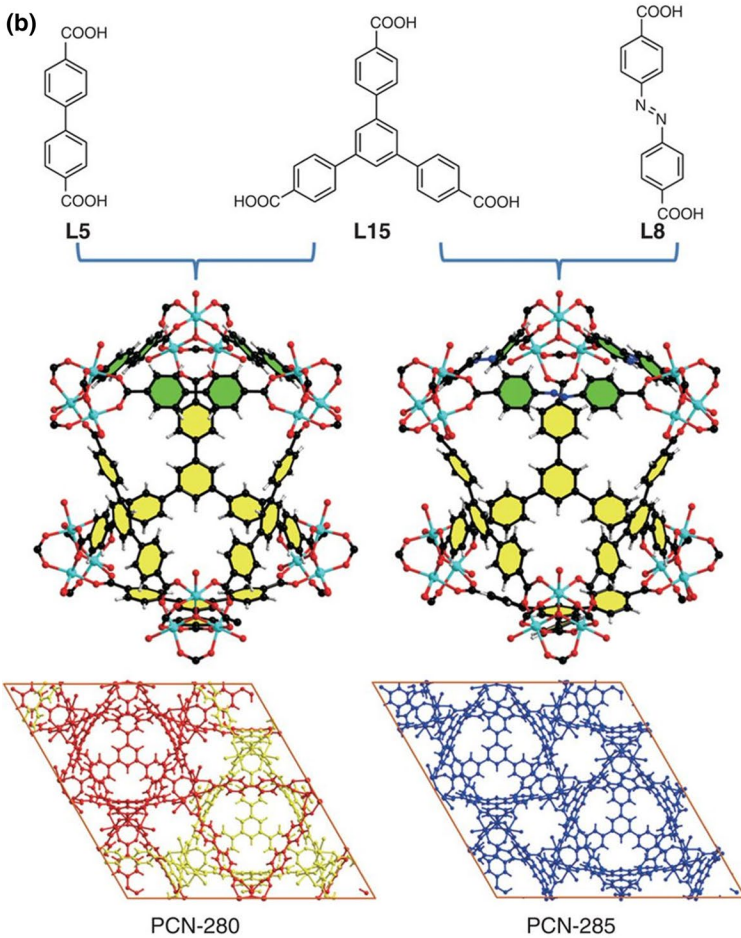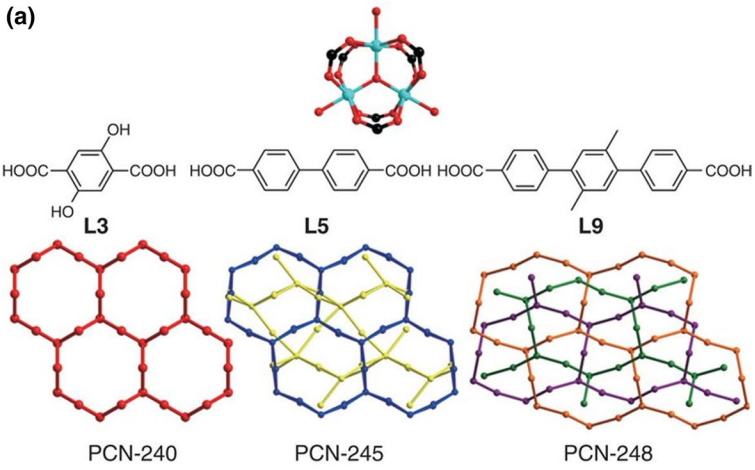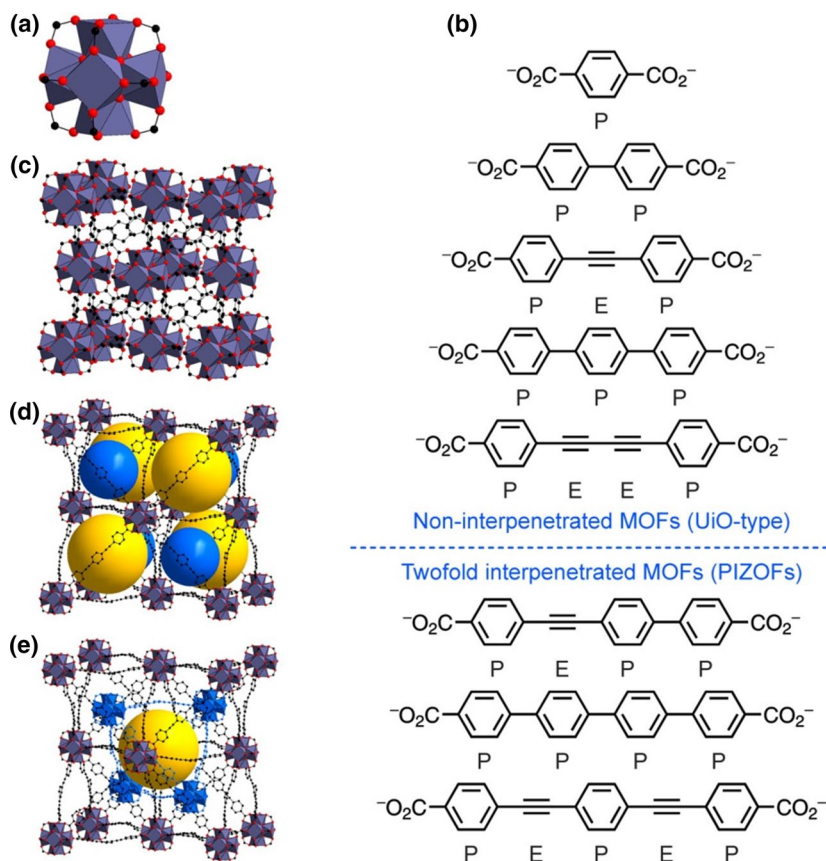
Fig. 16 Representation of the regulation of interpenetration using varying lengths of organic ligands constructed from phenylene (P) and ethynylene (E). Reproduced with permission from Ref. [70]

to the paddlewheel SBU (Fig. 19). Furthermore, the interpenetration also played a key role in the higher CO_2 selectivity over other gas such as N_2 and CH_4 with the Qst value for CO_2 (at zero coverage) ranging from 29 kJ mol^{-1} to 31 kJ mol^{-1} [115].

Shi et al. [116] prepared two luminescent metal organic frameworks **MOF-1** [Zn$_2$(L)$_2$(dpyb)] and **MOF-2** [Zn(L)(dipb)]·(H$_2$O)$_2$ based on π-conjugated thiophene-containing carboxylic acid ligand H$_2$L (3,3′-(thiophene-2,5-diyl)dibenzoic acid); dpyb = 1,4-di(pyridin-4-yl)benzene, dipb = 4,4′-di(1H-imidazol-1-yl)-1,1′-biphenyl. Both **MOF-1** and **MOF-2** showed twofold interpenetration; however, their networks and topological structures were completely different. In case of MOF-1, the Zn(II) paddlewheel SBUs are bridged by dbpyb ligands, giving rise to a 2D (4,4)-sql network having rhomb-like windows. The rhomb ring [Zn$_2$L$_2$] is further penetrated by dbpyb from an adjacent layer, resulting in a rotaxane structure that generates twofold entanglements (Fig. 20). Polyrotaxane entanglements of this type are rare.
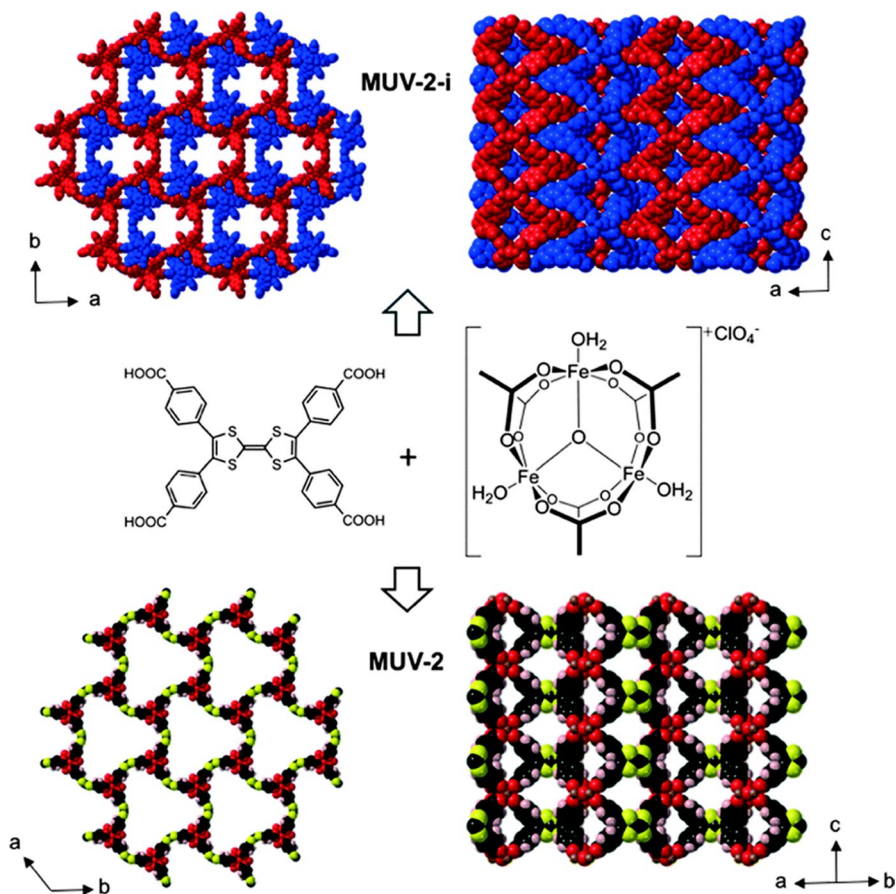
Fig. 17 Chemical structures of the ligand and of the $[Fe_3O(CH_3COO)_6]ClO_4$ secondary building unit used in the synthesis of **MUV-2-i** and **MUV-2**. Schematic representation of the crystal structures of **MUV-2-i** (the two interpenetrating nets colored *red* and *blue*) and **MUV-2** along the *c*-axis and perpendicular view of the structure. Reproduced with permission from Ref. [53]

	MOF	DOI	Reference
Table 2 Classical examples of metal–organic frameworks (MOFs) showing interpenetration. *DOI* Degree of interpenetration	$Cu(4,4'-bpy)_{1.5}NO_3(H_2O)_{1.25}$	Sixfold	[107]
	$Cu_3(BTB)_2(H_2O)_3 \cdot (DMF)_9(H_2O)_2$(MOF-14)	Twofold	[108]
	$Cu_3(TATB)_2(H_2O)_3$ (PCN-6)	Twofold	[109]
	$Zn_4O(C_{14}H_8O_4)_3$ (IRMOF-9)	Twofold	[110]
	$Zn_4O(C_{18}H_8O_4)_3$ (IRMOF-13)	Twofold	[110]
	$[Ni(bpe)_2(N(CN)_2)](N(CN)_2)(5H_2O)_n$	Twofold	[111]
	$(Yb_4(\mu_4-H_2O)(C_{24}H_{12}N_3O_6)_{8/3}$ $(SO_4)_2 \cdot 3\,H_2O \cdot 10\,DMSO)$ (PCN-17)	Twofold	[112]
	$[Zn_4O(bdc)_3]$ (IRMOF-1)	Twofold	[113]

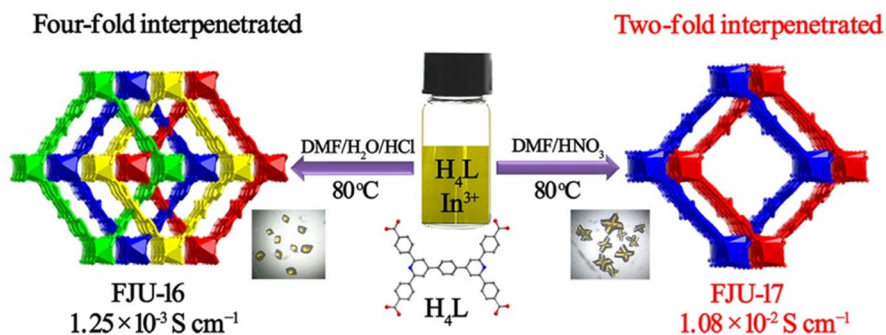**Fig. 18** Change of DOI in FJU-16 and FJU-17. Reproduced with permission from Ref. [114]

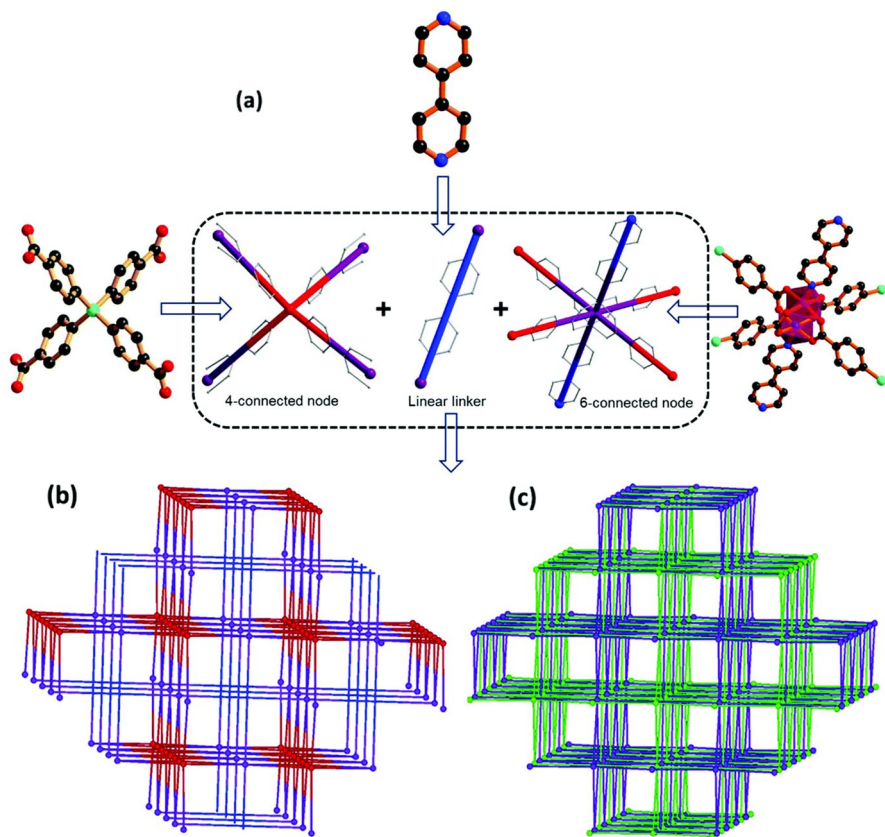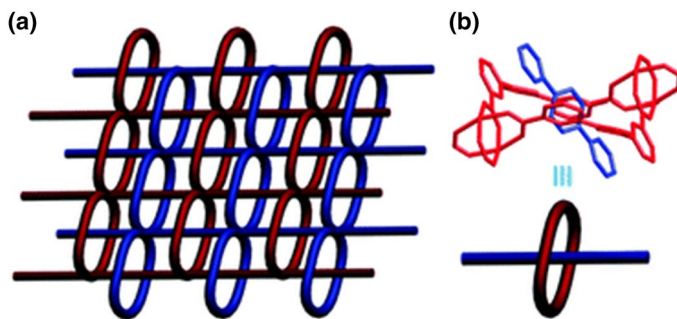**Fig. 19** **a** Simplified node and linker representation of the ligand L^{4-}, 4,4′-bipyridine and $Co_2(COO)_4$ cluster. **b** Representation of the (4,6)-connected two-nodal net, *sqc422* topology. **c** View of the twofold interpenetration into the framework. Reproduced with permission from Ref. [115]

Fig. 20 a Schematic representation of twofold interpenetrated layer structure of **MOF-1**. **b** Relative alignments of the wheel and axle in **MOF-1**. Reproduced with permission from Ref. [116]

In case of MOF-2, the binding of carboxylates is different in a mondodentate fashion and the dihedral angles between the thiophene and benzene rings of L are different from MOF-1 owing to free rotation of the C–C bond between the thiophene and benzene rings. MOF-2 displays the diamond (dia) topology with Schlafli symbol (6^6) and, as is the case with dia networks, the nets adopt twofold interpenetration to reduce the void space (Fig. 21).

Both MOF-1 and MOF-2 exhibited highly selective detection of picric acid through photoluminescence quenching [116].

4.2 Threefold

Tan et al. [117] reported on a nitrogen-containing threefold interpenetrated MOF, **SCUT-11**. Their work centered on the synthesis of a N-doped hierarchically mesoporous carbon (NHMC) catalyst via pyrolysis of **SCUT-11**. The triple interpenetration of **SCUT-11** provided high density Zn–O coordination units, encouraging the formation of mesopores with a bimodal pore size distribution. The properties of the interpenetrated MOF, such as mass transport of oxygen and increased accessibility of active sites, proved beneficial for catalysis, showing improved catalytic activity from previously reported MOFs. This carbon catalyst has potential
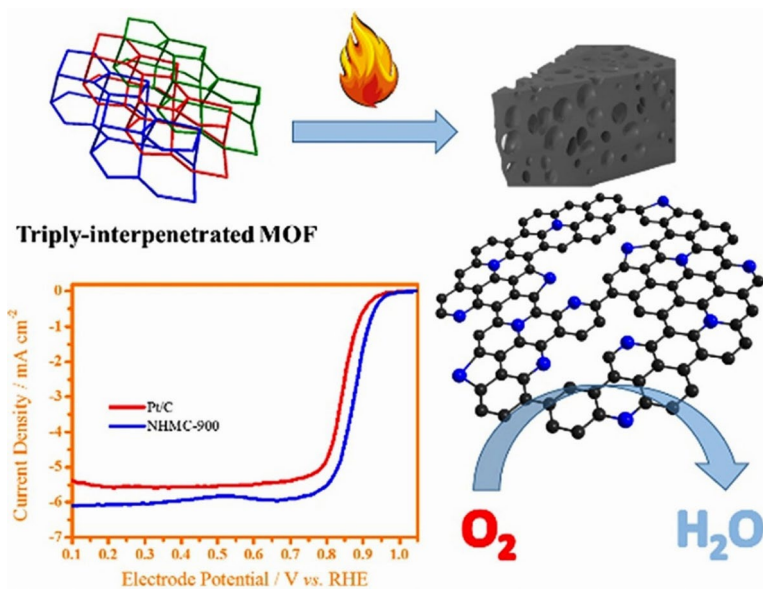
Fig. 21 Twofold interpenetrated dia topology of **MOF-2**. Reproduced with permission from Ref. [116]
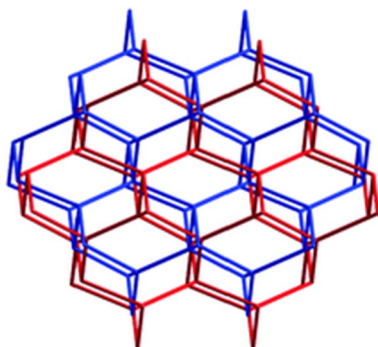
applications in fuel cells, being a non-Pt alternative to traditional expensive catalysts (Fig. 22) [117].

Liu et al. [118] reported a threefold interpenetrated MOF $[Zn_3(4,4'-ADB)_3(BIB)_2]_n$ based on mixed bridging ligands BIB and 4,4′-ADB [BIB = 1,4-bis(2-methyl-imi-dazol-1-yl)butane, 4,4′-ADB = azobenzene-4,4′-dicarboxylica acid]. The trinuclear Zn(II) SBUs are connected by 4,4′-ADB linker units forming a 2D layered structure with hexagonal pinwheel geometry. The BIB linkers connect the layer units above and below, generating a 3D hex net, which, in turn, interpenetrate to give threefold interpenetrated framework with $3^6 \cdot 4^{18} \cdot 5^3 \cdot 6$ topology (Fig. 23). The interpenetration reduces the effective void to 3.8% of the total volume but enhances the stability [118].

Wu et al. [119] obtained the first series of threefold interpenetrated uranium-organic frameworks UOF-1 and UOF-2 by utilizing semirigid carboxylic acids as the organic building blocks (H_3L1: 4,4′-[[2-[(4-Carboxyphenoxy)ethyl]-2-meth-ylpropane-1,3-diyl]dioxy]dibenzoic Acid for UOF-1; and H_6L2: Hexakis[4-(carboxyphenyl)oxamethyl]-3-oxapentane for UOF-2. In UOF-1, dimeric uranyl unit acts as the SBU linked by L1 forming a 3D network with large parallelogram channels, whereas, in UOF-2, the trimeric uranyl units acts as the SBU linked by L2 to give rise to the porous 3D framework having large channels. Owing to the large void volume in their single nets, both UOF-1 and UOF-2 undergo threefold interpenetration to stabilize the whole structure. UOF-1 is a 3,6-connected threefold interpenetrating net with flu topology whereas UOF-2 displays a four-connected net with pts topology (Fig. 24) [119].

Fig. 22 The triply interpenetrated MOF used as precursor for N-doped hierarchically mesoporous carbon (NHMC) synthesis. Reproduced with permission from Ref. [117]

Fig. 23 Threefold interpenetrating $3^6.4^{18}.5^3.6$ topology of **1**. Reproduced with permission from Ref. [118]
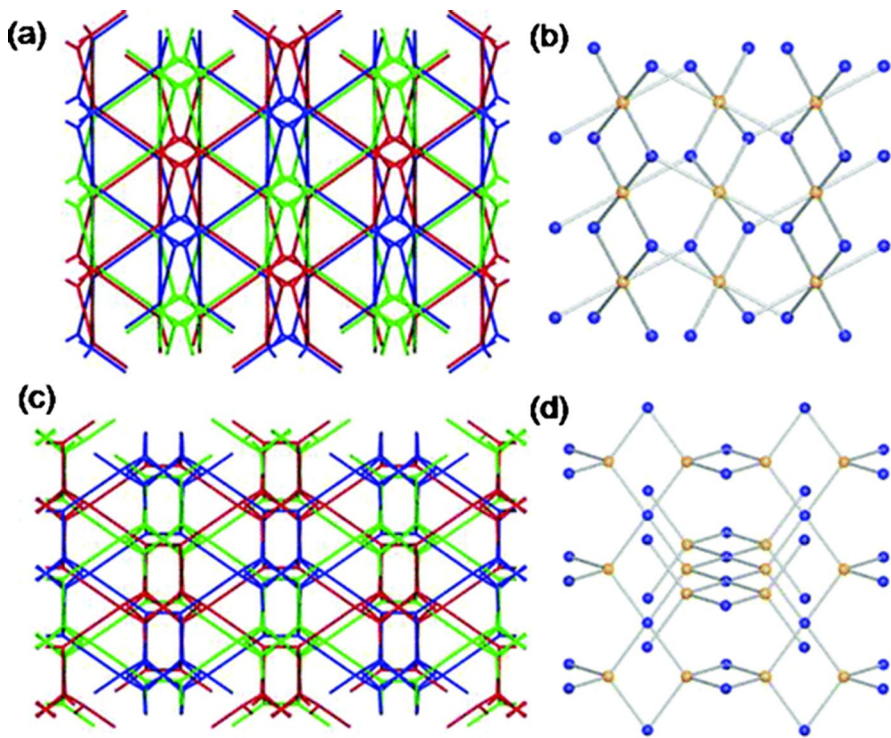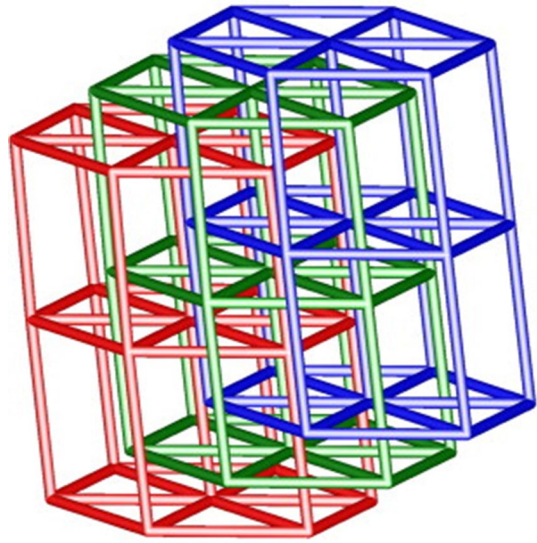
**Fig. 24** Simplified threefold-interpenetrated networks of **UOF-1** (**a**) and **UOF-2** (**c**) colored separately in *red*, *green*, and *blue*. Topological presentations of **UOF-1** (**b**) and **UOF-2** (**d**). Reproduced with permission from Ref. [119]

Mei et al. [120] further prepared a heterometallic uranyl-organic framework U-Ag-2,6-DCPCA from 2,6-dicholoroisonicotinic acid in the presence of uranyl and silver ions. The uranyl building unit having the combined influences of halogenation and the presence of silver ion additive on the uranyl coordination plays a major role in forming the threefold interpenetrated network. The halogen substitution alters the coordination mode of the isonicotinate ligand and through halogen–halogen interactions, stabilizes the threefold interpenetrating networks. The silver ions act as an inducer of uranyl species to tune the uranyl coordination. The uranyl building unit coordinated with six carboxylates shows further interaction with Ag^+ ions from four sides to give rise to a 2D (4,4)-connected network (Fig. 25). This heterometallic network can then interpenetrate to fill the huge void space in the 2D network leading to the threefold interpenetrated structure [120].

4.3 Fourfold

Zhu et al. [85] synthesized a Zn(II)-based MOF with fourfold interpenetration and *mog* topology (Fig. 26). This MOF showed an intense emission at 443 nm, with TNP (2,4,6-trinitrophenol), NFZ (nitrofurazone) and NFT (nitrofurantoin) efficiently quenching this luminescence. Nitroaromatics such as TNP are highly explosive and commonly used in industrial/civil explosives, creating hazardous pollution. NFZ and NFT are antibiotics that pose significant health hazards upon pollution into the environment due to antibiotic abuse. The quenching effect, attributed to both photo-electron induced transfer (PET) and fluorescence resonance energy transfer (FRET) mechanisms, is indicative of applications as a sensor for chemicals such as TNP, NFZ, and NFT [85].

Chen et al. [86] prepared a fourfold interpenetrated Cu(I) MOF ([Cu(pytpy)]. $NO_3.CH_3OH)_n$ from $Cu(NO_3)_2 \cdot 3H_2O$ with 2,4,6-tris(4-pyridyl)pyridine (pytpy) in
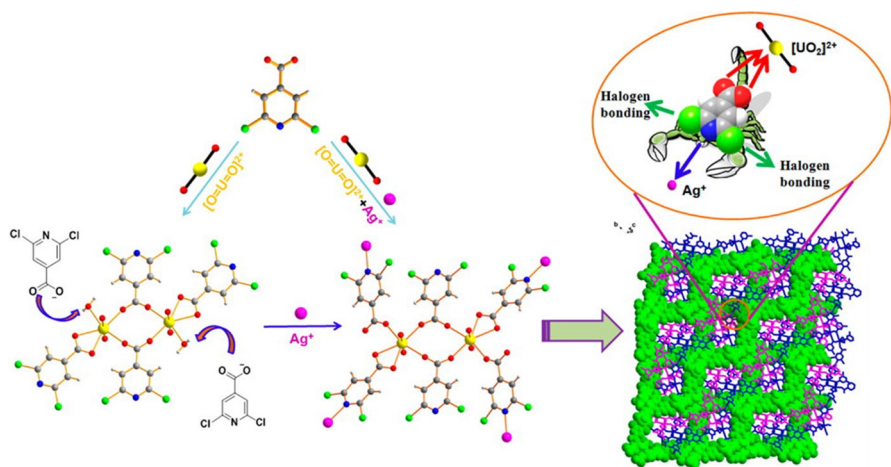
Fig. 25 Heterometallic interpenetrating network found in U-Ag-2,6-DCPCA and Halogen–halogen interactions found between adjacent layers. Reproduced with permission from Ref. [120]
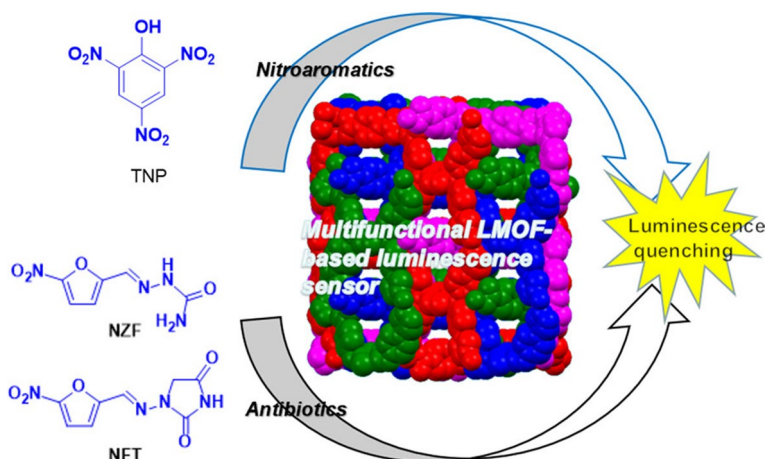
Fig. 26 The multifunctional Zn(II)-based fourfold interpenetrated MOF for sensitive sensing of TNP, NFT and NZF. Reproduced with permission from Ref. [85]

mixed-solvent. The Cu(I) ion and pytpy act as three-connected nodes displaying an unusual unimodal (10,3)-*b* topology which can also be denoted as ThSi$_2$. The large void space in the network and self-dual nature of the ThSi$_2$ topology lead to four individual nets interpenetrating with each other and give rise to a cationic 3D framework with helical channels (Fig. 27). Moreover, water molecules could replace the guest methanol molecules in the channels of the framework, and the resulting
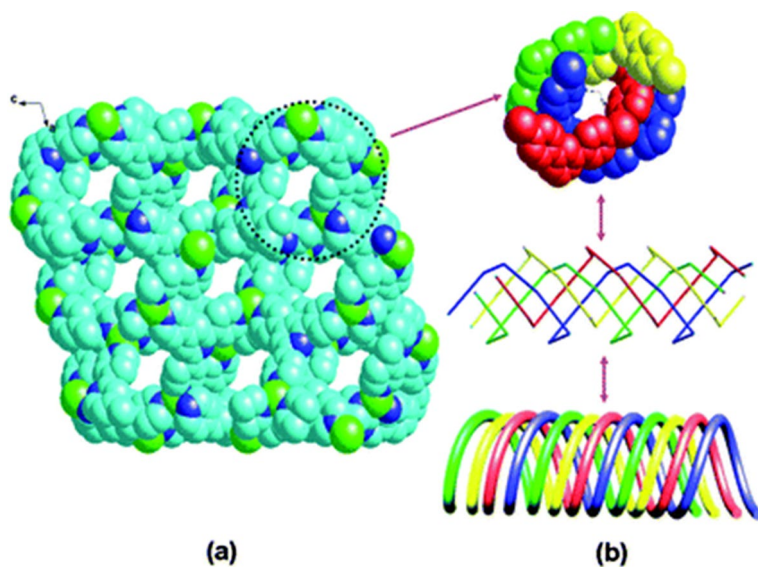
Fig. 27 **a** Space-filling diagram of the fourfold interpenetration in **1** viewed along the *b* axis (solvent molecules and nitrate anions omitted). **b** Views of the single fourfold helical channel. Reproduced with permission from Ref. [86]

hydrated complex could serve as a host for anions displaying different geometries. The desolvated complex also showed selective CO_2 uptake over N_2 at room temperature [86].

Zhang et al. [121] utilized a fourfold interpenetrated MOF, $[Ni(pybz)_2]$ (pybz = 4-(4-pyridyl)- benzoate) with dia topology as a coating material in gas chromatographic capillary column to separate low boiling point essential oils. The extra structural stability through the fourfold interpenetration, weak molecular interacting sites in the ligand in form of aromatic rings and polarized C–O/C=O groups and strained chelating carboxylate groups coordinated to the metal center, which can show interaction with adsorbate molecules to relieve the strain rendered it as a good stationary phase material (Fig. 28). The fourfold interpenetrated network facilitated the passing of the analysts through the pores because of the 1D square channels with window size of 7.6 Å × 7.6 Å which was larger or close to kinetic minimum cross-sectional diameter of the analytes [121].

4.4 Fivefold

Wen et al. [87] reported a unique polythreaded MOF with five-fold interpenetration with *mot* topology (Fig. 29). The authors noted the thermal stability of the MOF, stable up to temperatures of ca. 273 °C, characteristic of higher degrees of interpenetrated frameworks. The MOF also remained stable in air under ambient conditions and retained its crystalline structure. The structure was able to be fine-tuned as a result of the long, flexible ligands and the reaction sensitivity to pH and temperature [87].

Wei et al. [88] reported two isostructural five-fold interpenetrated dia MOFs $[M(bpg)(bdc).2H_2O]$ (M = Zn(II), Cd(II); bpg = meso-α,β-bi(4-pyridyl) glycol and
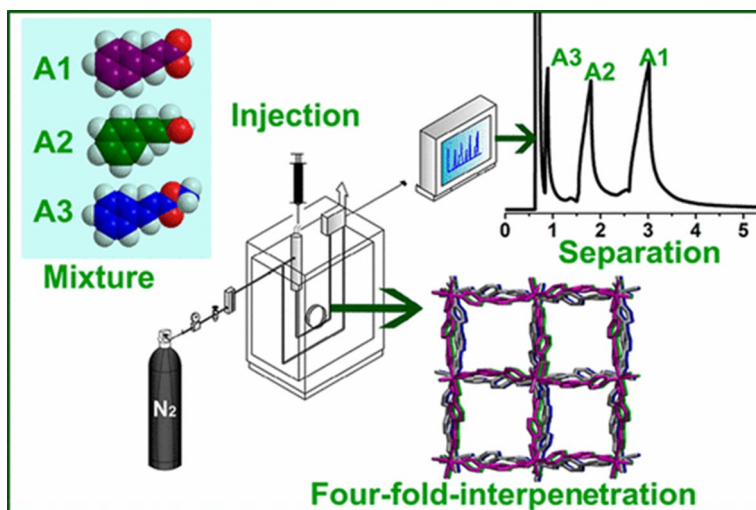
Fig. 28 The utilization of fourfold interpenetrated [Ni(pybz)2] as a coating material in the gas chromatographic capillary column. Reproduced with permission from Ref. [121]
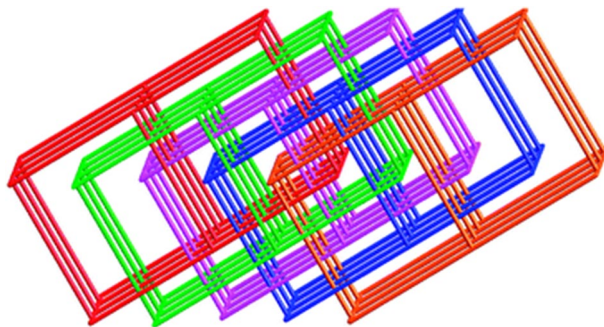
Fig. 29 Schematic view of the fivefold interpenetrated MOF. Reproduced with permission from Ref. [87]

$H_2bdc = 1,4$-benzenedicarboxylic acid). These are rare examples of five-old interpenetrated MOFs with mixed organic ligands of different lengths. This fivefold parallel interpenetration structure could be categorized as five topologically equivalent 3D subsets related by the translation vector [1, 0, 0]. The overall structure can be seen as a 4-c diamond framework with large hexagonal channel that allows for the penetration of each net by four other nets (Fig. 30). The frameworks could still retain effective void volume of 11.6% and 10.1% (of crystal volume) for the Cd-MOF and the Zn-MOF, respectively [88].

A fivefold interpenetrated MOF exhibiting colossal uniaxial negative thermal expansion (NTE) was reported by Aggarwal et al. [122]. The ([Zn(FMA)(BPA)] $H_2O)_n$ (**1·H$_2$O**) (FMA2 = fumarate, BPA = 1,2-bis-(4-pyridyl)ethane) exhibited a unique mode of interpenetration consisting of two sets of nets, one being twofold interpenetrated and the other being threefold interpenetrated. It is generally expected that the presence of extra networks acting as barriers to transverse vibrations due to interpenetration could decrease or suppress the NTE. However, the combined effect of hinge-like motion and the sliding of individual diamondoid networks led to the anomalous thermal expansion behavior (Fig. 31). The frameworks **1** and **1·H$_2$O** are a new class of thermoresponsive interpenetrated MOFs exhibiting anomalous NTE [122].

4.5 Sixfold

Zhang et al. [123] reported a sixfold interpenetrated MOF with 3D diamondoid nets (Fig. 32). Through luminescence measurements, the MOF was shown to have selective sensing properties, specifically for Fe^{3+} cations in aqueous solution, and nitrobenzene derivatives nitrobenzene, *p*-nitrotoluene, *p*-nitroaniline and *p*-nitrophenol in DMF. These nitroaromatics and metal cations had a quenching effect of the luminosity of the MOF. These properties are promising for functional applications in chemical sensors [123].

Zhao's group reported a Zn-MOF ([Zn(XL)2](ClO$_4$)2·6H$_2$O)n (XL = *N,N'*-bicyclo[2.2.2]oct-7-ene-2,3,5,6-tetracarboxdiimidebi(1,2,4-triazole)) with six-fold interpenetration that displayed high thermal stability and solvent stability [124].
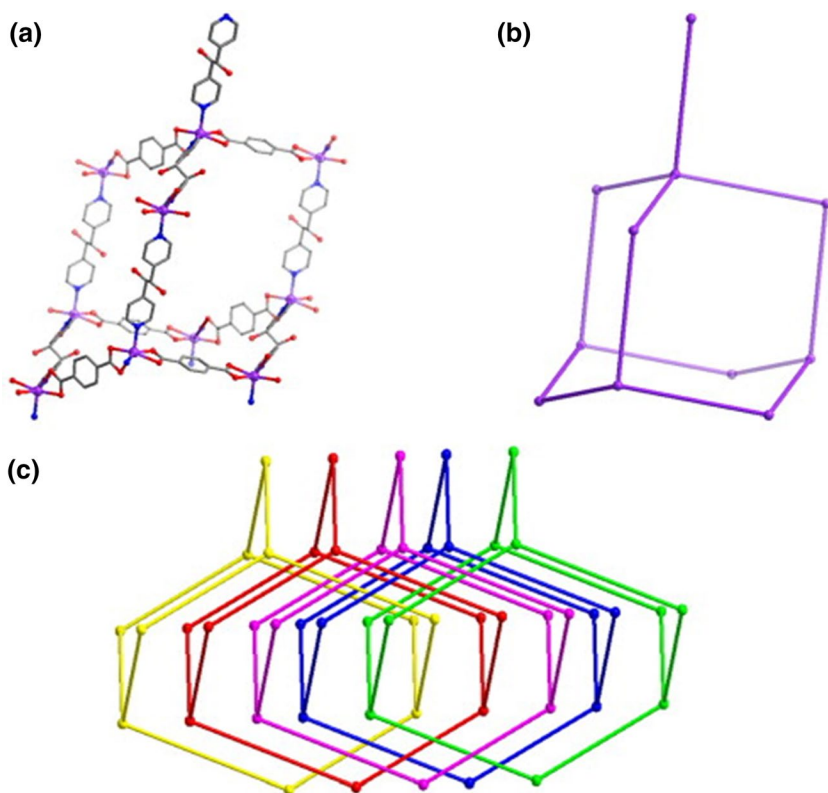
Fig. 30 a Perspective view of the single diamond net. **b** Simplified view of the single diamond net. **c** Schematic representation of the fivefold interpenetrating 3D diamond net. Reproduced with permission from Ref. [88]

This is the first example of sixfold interpenetrating network having the sqc6 topology with an unusual [2+2+2] mode of interpenetration (Fig. 33). The framework could further act as a luminescent sensor for highly sensitive and selective detection of acetylacetone with the detection limit of 1.72 ppm [124].

4.6 Sevenfold

Song et al. [125] reported a sevenfold interpenetrated MOF with a unique structure of pseudo-helical chains and a unique catenane-like motif with Hopf links (Fig. 34). Upon luminescence experiments, this MOF shows an intense emission at 405 nm. The intensity may be attributed to the $\pi^* \rightarrow \pi$ transitions of the ligand, enhanced by coordination to the metal center. Preliminary experiments indicated that this compound may be an excellent candidate for photoactive materials [125].

Li et al. [126] synthesized a sevenfold interpenetrated framework exhibiting amine selective chemochromism, thermochromism, electrochromism and X-ray and UV dual photochromism. The $[Zn_7(bpybc)_3(o\text{-}BDC)_6] \cdot 2NO_3 \cdot 6H_2O$
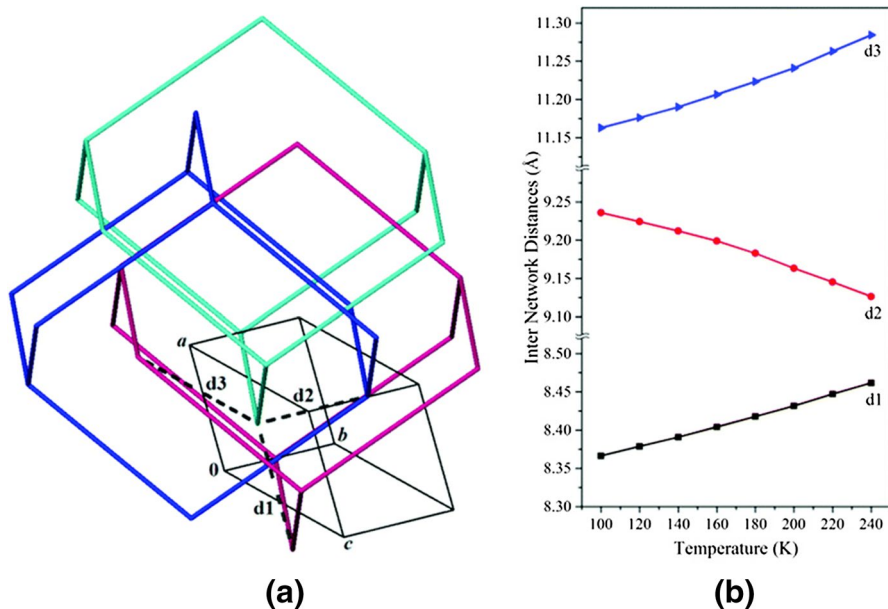
**Fig. 31 a** View of various internetwork distances along the crystallographic *a*, *b* and *c* axes (only three interpenetrated networks are shown for clarity). **b** Changes in the inter-network distances with temperature **1·H₂O**. Reproduced with permission from Ref. [122]

(bpybc = 1,1′-bis(4-carboxyphenyl)-4,4′-bipyridinium, o-BDC = o-benzenedicarboylic acid) featured unique Anderson-like metal carboxylate clusters and the six-connected Zn_7 SBU and bpybc ligand generated a 3D pcu network (Fig. 35). The framework retained its porosity despite the sevenfold interpenetration with potential void spaces estimated at 20.6% per unit volume. The authors followed the strategy to incorporate the viologen derivatives into metal carboxylate clusters, and to assemble the interpenetrating motif to form multibridges for electron transfers and stabilize the reduced radicals. The short distances between the donor–acceptor, multipathways for electron transfer and stabilization of the radicals endowed the framework with response to the various stimuli of heat, electricity, UV-light, soft X-ray and some organic amines. Moreover, the high stability and good reversibility make it an excellent smart material for practical application [126].

4.7 Eightfold

The eightfold interpenetrated MOF [**Cd(L)₂**, L = (E)-4-(2-(1Himidazol-4-yl)vinyl) benzoic acid] contains a 3D dia network with (6^6) topology (Fig. 36). The thermal stability of this highly interpenetrated MOF was noted, with no weight loss evident until 400 °C. The optical properties of this complex were investigated as non-centrosymmetric structures can have second-order non-linear optical (NLO) effects. When compared with urea, the complex gave off 1.4 times the strong powder second
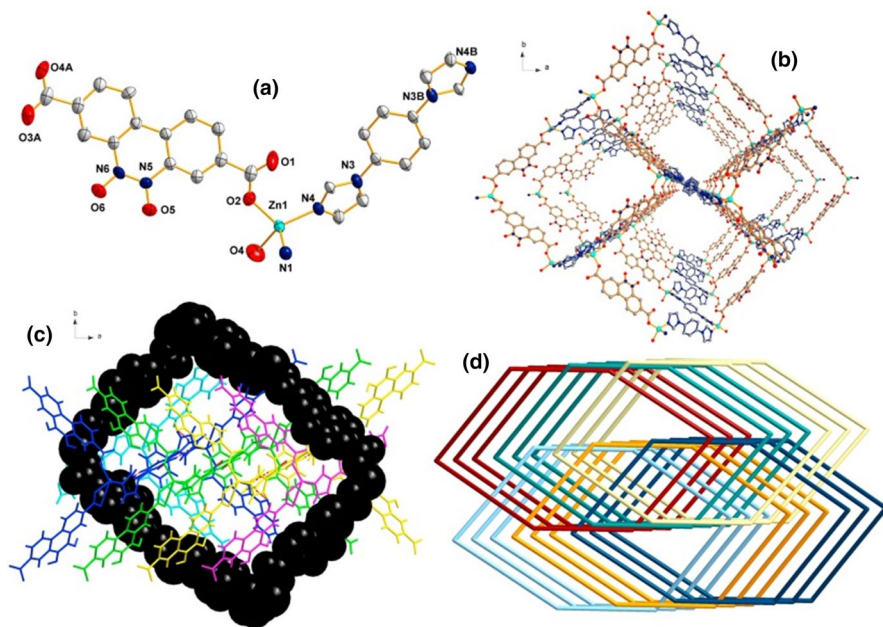
Fig. 32 a The asymmetric unit of **2**. **b** The central projection diagram of **2** views along *c* axis. **c** The six-fold interspersed microporous structure of compound **2**. **d** Sixfold 3D→3D 4-connected (6^6) **dia** topology in compound **2**. Reproduced with permission from Ref. [123]

harmonic generation (SHG) intensity, confirming the suspected NLO effects. The MOF also showed strong fluorescence, indicative of applications in chemical sensing [127].

Chen et al. [128] reported the structural transformation of a 7-fold interpenetrated MOF to 8-fold interpenetrated MOF (Fig. 37) upon loss of the DMF molecules in a SCSC fashion. The $[Zn(pvb)_2]\cdot DMF$ (1) and $[Zn(pvb)_2]$(2) (pvb = trans-2-(4-pyridyl)-4-vinylbenzoate) showed dia topology with sevenfold and eightfold interpenetrations, respectively. The authors observed that the alternating dia fragments from adjacent layers start moving towards each other to reduce the void space upon removal of the guest DMF molecules. The Zn(II)-ligand bonds broke during these movements and reformed, which led to an increase in interpenetration. This change in interpenetration brought the dia nets closer, which facilitated the interactions between them and led to a giant enhancement of SHG, useful for tuning non-linear optical (NLO) properties [128].

4.8 More Than Eightfold Interpenetration

Examples of MOFs with DOI more than eightfold are relatively few, and with an increase in the DOI, the pore size tends to decrease, which could make the interpenetrating MOFs nonporous.
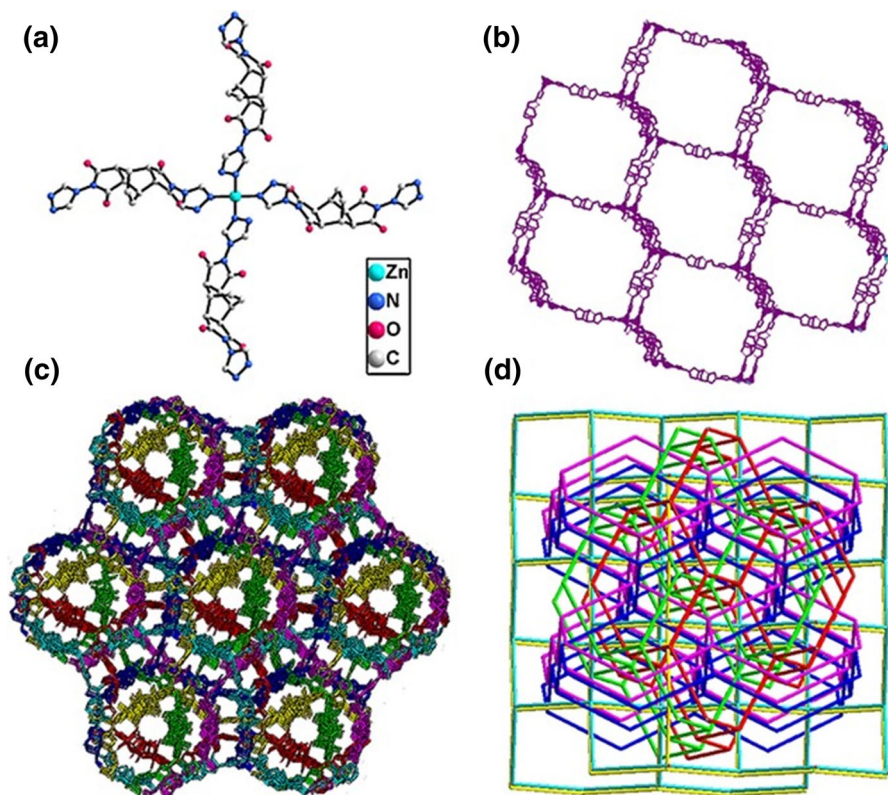
Fig. 33 **a** Coordination environment of Zn^{2+}. **b** Set of interpenetrating framework of **1**. **c** View of 3D structure of **1**. **d** Topological representation of sixfold interpenetrating structure from three sets of two-fold interpenetrating network. Reproduced with permission from Ref. [124]

Tseng et al. [129] reported a huge diamondoid MOF featuring tenfold interpenetrating neo-mode. The di-*tert*-butyl-4,10-dihydropyreno[4,5-*d*:9,10-*d'*]diimidazole-5,11-diyl)dibenzoic acid), featuring a huge and nearly undistorted adamantine cage and an extra-framework volume of up to 48.7%. Despite the high DOI, **1** still features small pore openings having dimensions of 4.5×3 Å^2 and 2×1.5 Å^2 along the a and b axes. There are five paired sets of twofold mutually interpenetrated dia nets and the topology is unique tenfold in [2+2+2+2+2] mode (Fig. 38). The framework, however, did not show significant nitrogen adsorption [129].

Loukopoulos et al. [130] reported a 12-fold interpenetrated ThSi$_2$ (ths) topology framework [Cu$_3$(L1)$_2$(H$_2$O)$_8$]·8H$_2$O utilizing glycine based tripodal pseudopeptidic ligand H$_3$L = *N,N',N''*-tris(carboxymethyl)-1,3,5-benzenetricarboxamide or trimesoyl-tris–glycine. Each metal center acts as a two-connected node, with each ligand as a three connected-node to generate three connected, 12-fold interpenetrated symmetric ths net (Fig. 39). The choice of the Cu(II) starting material can play an important role in the self-assembly of the final product. The framework was further
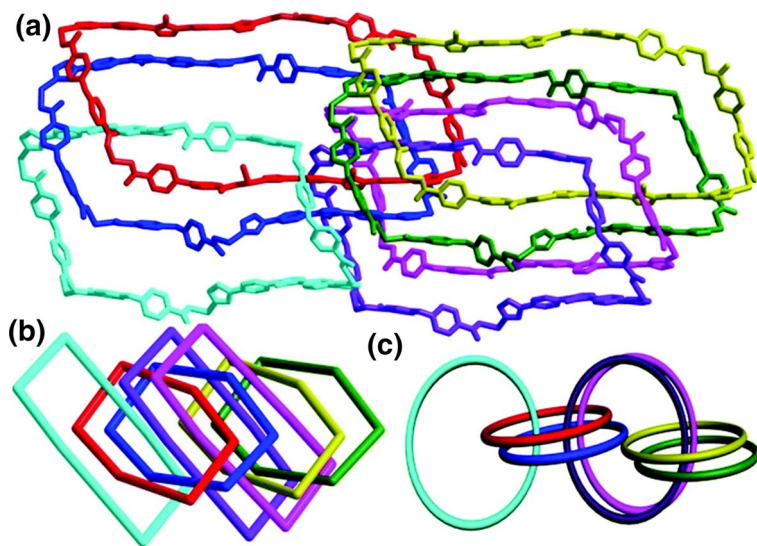
Fig. 34 **a** Exceptional catenane-like motifs are catenated through novel polycatenane Hopf links in **1**. **b**, **c** Schematic representation of the polycatenane characters in **1** Reproduced with permission from Ref. [125]

utilized for multicomponent synthesis of propargylamines under mild conditions, and showed good catalytic activity [130].

The highest DOI reported so far has been by Wu et al. [131], who demonstrated record 54 interpenetrating networks in the framework $Ag_3(OH)(H_2O)_2(Tipa)_{2.5}]$ $[Mo_2O_7]\cdot4.5H_2O$ (**1**; Tipa = tri(4-imidazolylphenyl)amine), which has three-connecting ligands and two-connecting metal ions. The authors hypothesized the strategy of having metal ions coordinating to only two polydentate ligands, leading to longer links between nodes increasing the ring sizes. Another strategy proposed was to target networks with three-connecting nodes since lower connectivity nets could give rise to more open frameworks. This interpenetration belongs to the rare class IIIb with 10^3-srs topology. There are two sets of nine nets of opposite chirality, and each set could be generated by the translation of one net along two of the three fourfold helix axes but not along the third (Fig. 40) [131] (Scheme 3).

4.9 Partial Interpenetration

Over the past couple of years, an interesting phenomenon of partial interpenetration has been observed, whereby one framework is partially occupied inside of the second framework Scheme 1). Schroder's group first observed that the partially interpenetrated **NOTT-202** contains a dominant lattice and a slower-forming secondary lattice. The development of the secondary lattice determines the level of partial interpenetration of the resulting MOF (Fig. 41). Partially interpenetrated
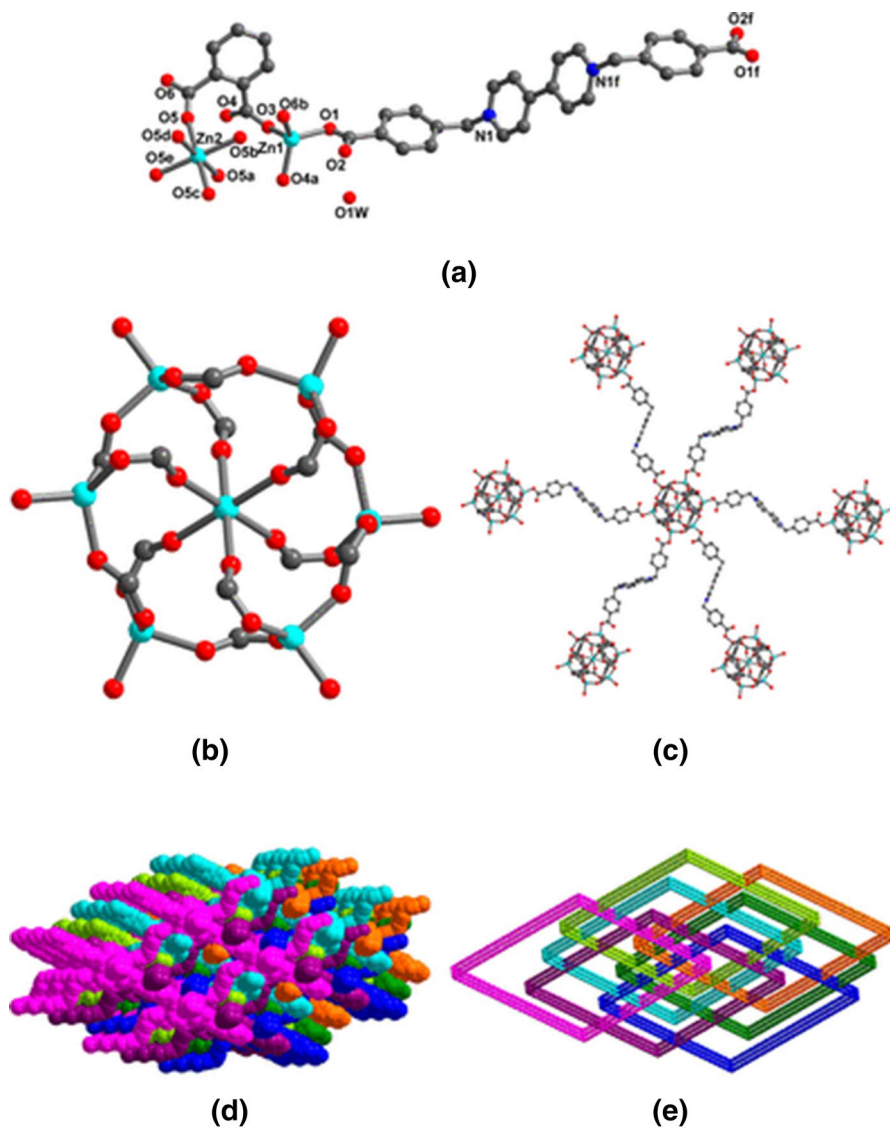
Fig. 35 **a** Coordination environments of the Zn^{2+} ion. **b** View of $Zn_7O_{30}C_{12}$ cluster (Anderson-like type), **c** Zn_7 Anderson-like cluster linked by six bpybc ligands. **d** Space-filling view of the sevenfold interpenetration of **pcu** primitive cubic framework. **e** Schematic diagram of the 7-fold interpenetration for **1**. Reproduced with permission from Ref. [126]

MOFs show special applications in selective gas sorption due to both the capacity and selectivity. While the large, non-interpenetrated pores allow for rapid diffusion, the smaller interpenetrated pores are able to selectively capture smaller gas molecules. **NOTT-202a** (the solvated form of **NOTT-202**) was reported having
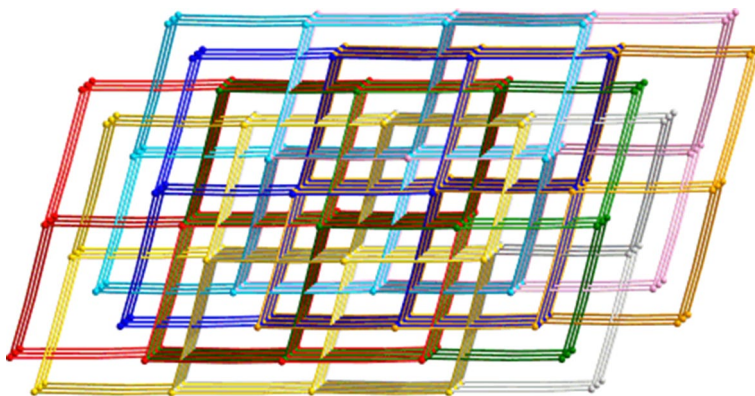
Fig. 36 Schematic representation of the eightfold interpenetrating [Cd(L)2]. Reproduced with permission from Ref. [127]

(a)   **(b)**
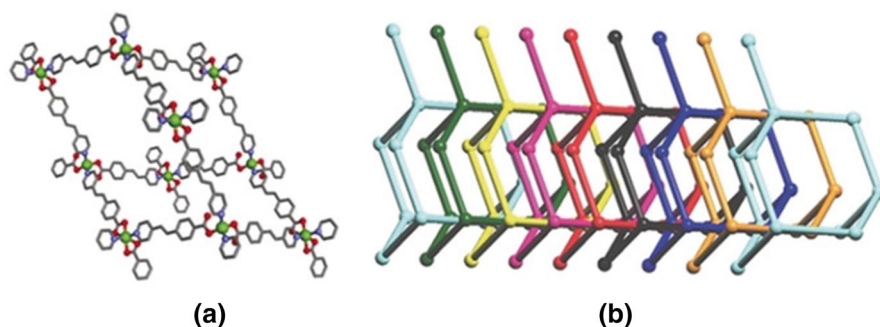
Fig. 37 **a** A view of the **dia** net in **2**. *Green* Zn, *red* O, *blue* N, *gray* C. **b** The eightfold interpenetrated nets in **2**. Reproduced with permission from Ref. [128]

the highest BET surface area and CO_2 storage capacity for a MOF containing In(III) [132].

Ferguson et al. [133] expanded this further and were able to control the degree of partial interpenetration as described in the section Solvent System.

The research group of Ma [133] also observed the presence of partial interpenetration in $[Cu_2(pbpta)(2H_2O)) \cdot (Cu_2(pbpta)(2H_2O))_{0.5} \cdot (Cu_2(pbpta)(2H_2O))_{0.25}]_n$, whereby the parent framework (1) was fully occupied, and the latter two showed

Fig. 38a–c Structures of **1**. **a** A huge adamantane cage and its simplification. **b** Perspective view of ten▶ individually entangled adamantane cages along the *c* axis (only the main aromatic skeleton is shown for clarity). **c** Side stereoview of part **b**, **d** a simplified pattern of part **b**. Reproduced with permission from Ref. [129]

(a)

(d)

(b)

(c)
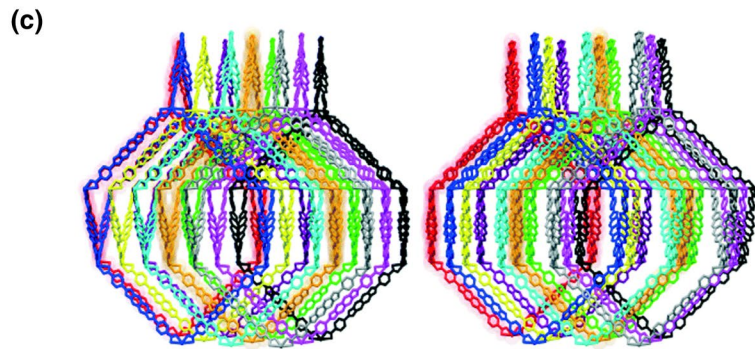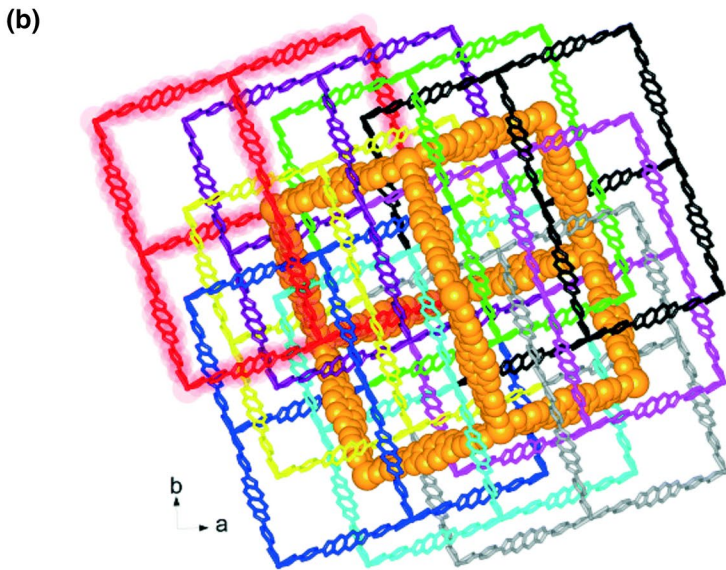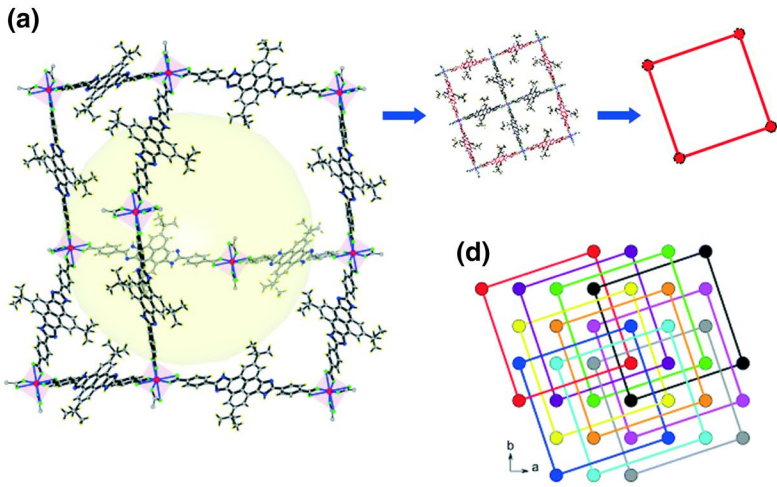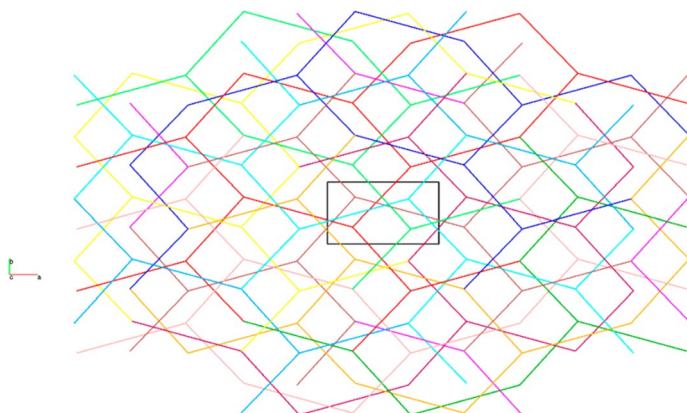
Fig. 39 Simplified colored versions of the 3D 12-fold interpenetrated **ths** network found in **1** along the *b0a* planes. Reproduced with permission from Ref. [130]

occupancies of 50% (2) and 25% (3) shown in Fig. 42. The framework exhibited NbO topology and showed good separation capability for CO_2 over CH_4 [133].

Recently, the Zaworotko group [134] also reported a control over the degree of partial interpenetration by controlling the temperature and concentration for a twofold hybrid ultramicroporous material (HUM), **SIFSIX-14-Cu-I** with pcu topology (Fig. 43). Phases with 99%, 93%, 89%, and 70% partial interpenetration were obtained and with a decrease in proportion of the interpenetrated component, the C_2H_2/C_2H_4 separation performance decreased [134].

5 Conclusions

Interpenetration in MOFs has been widely reported on with the desired functional applications. An increasing number of examples in the literature highlight the importance of understanding the synthetic factors that can help modulate the resulting frameworks. Factors such as temperature, solvent system, time duration and linker design play an important role in regulating the DOI in MOFs. Generally, higher temperatures, less bulky solvents and an increased time duration for synthesis lead to a higher DOI. Less steric bulk and elongated ligand length also contribute to an increase in DOI. Conversely, lower temperatures, smaller time durations and bulky solvents favor non-interpenetrated or less interpenetrated frameworks. Ligands with groups having steric repulsions and shorter lengths can be used as controls for reduced DOI because of the smaller void space available for other networks to fit into. This understanding can assist in the design of new materials that balance the trade-offs of structural stability and high storage capacities, leading to advanced materials with the desired applications. Many
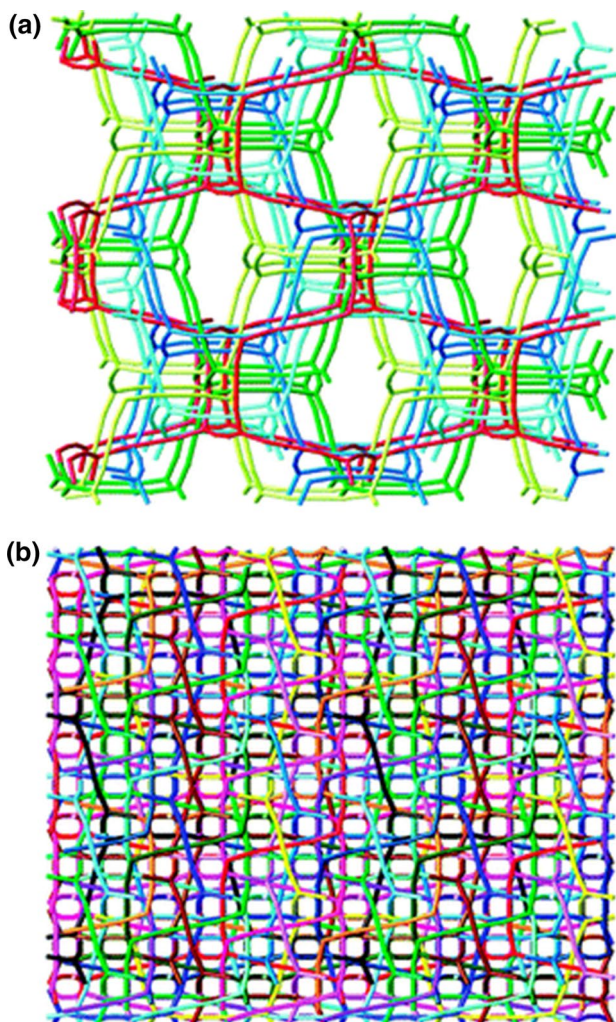
Fig. 40 **a** Interpenetration of four nets of one handedness (*green/blue* nets) with one of the opposite handedness (*red*). **b** Interpenetration of all 54 networks. Reproduced with permission from Ref. [131]

advantageous properties, such as selective guest capture, stepwise guest adsorption, enhanced framework robustness, photoluminescence control, and guest responsive porosity have arisen due to the presence of interpenetration in MOFs. More insights are needed into understanding the growth mechanisms of the formation of interpenetrated structures based on kinetic/thermodynamic controls. Further exploration of the functional applications of interpenetrated MOFs should be directed towards catalysis, sensing, gas uptake and separation, among others.
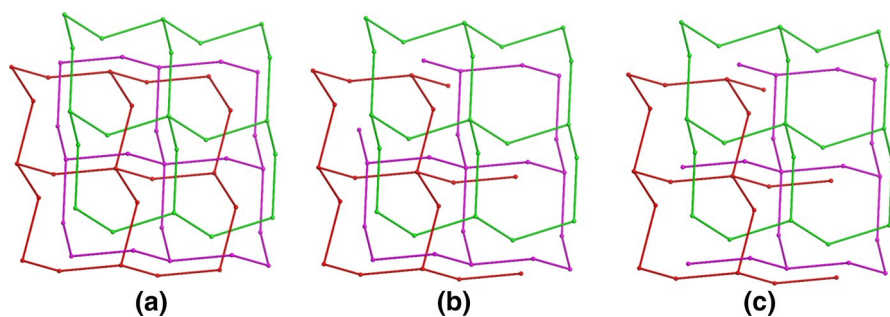
Scheme 3a–c Depiction of partial interpenetration in a threefold interpenetrated dia-MOF. **a** Full occupancy of the three nets. **b**, **c** Fully occupied *green* net and partially occupied *red* and *pink* nets
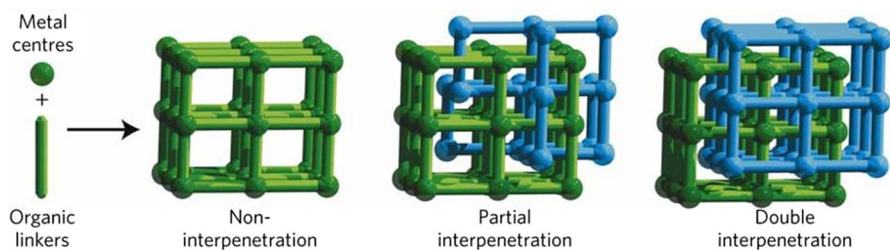
Fig. 41 Representation of the formation of interpenetrated and partially interpenetrated MOFs, consisting of a dominant lattice and a slower-forming secondary lattice. Reproduced with permission from Ref. [132]
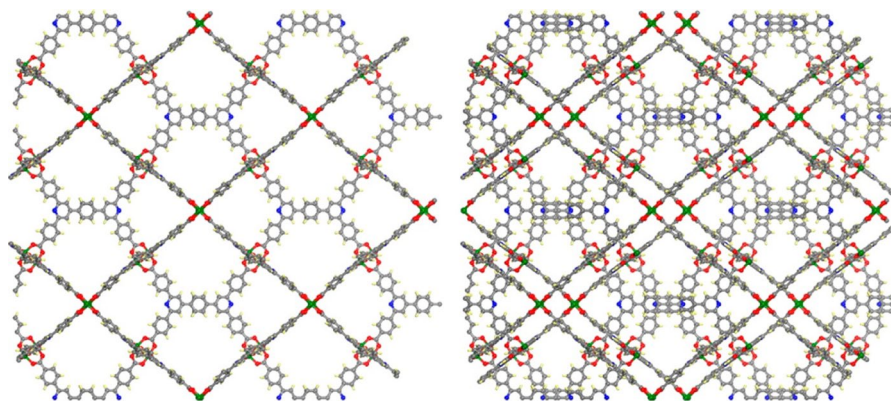
Fig. 42 Non-interpenetrated and interpenetrated view along the *z*-axis. Reproduced with permission from Ref. [133]

Fig. 43 Different phases obtained with a change in partial occupancy. Reproduced with permission from Ref. [134]
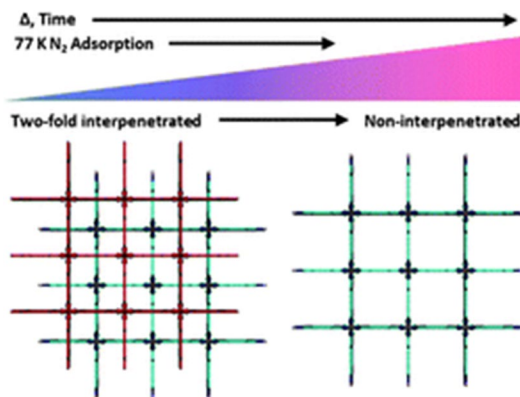
References

1. Zhou H-C, Long JR, Yaghi OM (2012) Introduction to metal–organic frameworks. Chem Rev 112:673–674
2. James SL (2003) Metal–organic frameworks. Chem Soc Rev 32:276–288
3. Meek ST, Greathouse JA, Allendorf MD (2011) Metal–organic frameworks: a rapidly growing class of versatile nanoporous materials. Adv Mater 23:249–267
4. Gharib M, Safarifard V, Morsali A (2018) Ultrasound assisted synthesis of amide functionalized metal–organic framework for nitroaromatic sensing. Ultrason Sonochem 42:112–118
5. Zhang Z, Yang Q, Cui X, Yang L, Bao Z, Ren Q, Xing H (2017) Sorting of C4 olefins with interpenetrated hybrid ultramicroporous materials by combining molecular recognition and size-sieving. Angew Chem Int Ed 56:16282–16287
6. Batten Stuart R, Champness Neil R, Chen X-M, Garcia-Martinez J, Kitagawa S, Öhrström L, O'Keeffe M, Paik Suh M, Reedijk J (2013) Terminology of metal–organic frameworks and coordination polymers (IUPAC recommendations 2013). Pure Appl Chem. https://doi.org/10.1351/PAC-REC-12-11-20
7. MacGillivray LR (2010) Metal–organic frameworks: design and application. Wiley, New York
8. Stock N, Biswas S (2012) Synthesis of metal–organic frameworks (MOFs): routes to various MOF topologies, morphologies, and composites. Chem Rev 112:933–969
9. Cook TR, Zheng Y-R, Stang PJ (2013) Metal–organic frameworks and self-assembled supramolecular coordination complexes: comparing and contrasting the design, synthesis, and functionality of metal–organic materials. Chem Rev 113:734–777
10. Cheong VF, Moh PY (2018) Recent advancement in metal–organic framework: synthesis, activation, functionalisation, and bulk production. Mater Sci Technol 34:1025–1045
11. Kalmutzki MJ, Hanikel N, Yaghi OM (2018) Secondary building units as the turning point in the development of the reticular chemistry of MOFs. Sci Adv 4:eaat9180
12. Lu W, Wei Z, Gu Z-Y, Liu T-F, Park J, Park J, Tian J, Zhang M, Zhang Q, Gentle Iii T, Bosch M, Zhou H-C (2014) Tuning the structure and function of metal–organic frameworks via linker design. Chem Soc Rev 43:5561–5593
13. Furukawa H, Cordova KE, O'Keeffe M, Yaghi OM (2013) The chemistry and applications of metal–orrganic frameworks. Science 341:1230444
14. Kirchon A, Feng L, Drake HF, Joseph EA, Zhou H-C (2018) From fundamentals to applications: a toolbox for robust and multifunctional MOF materials. Chem Soc Rev 47:8611–8638

15. Lin Z-J, Lü J, Hong M, Cao R (2014) Metal–organic frameworks based on flexible ligands (FL-MOFs): structures and applications. Chem Soc Rev 43:5867–5895

16. Yuan S, Feng L, Wang K, Pang J, Bosch M, Lollar C, Sun Y, Qin J, Yang X, Zhang P, Wang Q, Zou L, Zhang Y, Zhang L, Fang Y, Li J, Zhou H-C (2018) Stable metal–orrganic frameworks: design, synthesis, and applications. Adv Mater 30:1704303

17. Ding M, Flaig RW, Jiang H-L, Yaghi OM (2019) Carbon capture and conversion using metal–organic frameworks and MOF-based materials. Chem Soc Rev 48:2783–2828

18. Hendon CH, Rieth AJ, Korzyński MD, Dincă M (2017) Grand challenges and future opportunities for metal–orrganic frameworks. ACS Cent Sci 3:554–563

19. Ricco R, Pfeiffer C, Sumida K, Sumby CJ, Falcaro P, Furukawa S, Champness NR, Doonan CJ (2016) Emerging applications of metal–organic frameworks. CrystEngComm 18:6532–6542

20. Tansell AJ, Jones CL, Easun TL (2017) MOF the beaten track: unusual structures and uncommon applications of metal–organic frameworks. Chem Cent J 11:100

21. Allendorf MD, Stavila V (2015) Crystal engineering, structure–function relationships, and the future of metal–organic frameworks. CrystEngComm 17:229–246

22. Wu D, Yang Q, Zhong C, Liu D, Huang H, Zhang W, Maurin G (2012) Revealing the structure–property relationships of metal–orrganic frameworks for CO_2 capture from flue gas. Langmuir 28:12094–12099

23. Alkordi MH, Belmabkhout Y, Cairns A, Eddaoudi M (2017) Metal–orrganic frameworks for H_2 and CH_4 storage: insights on the pore geometry-sorption energetics relationship. IUCrJ 4:131–135

24. Fang Z, Dürholt JP, Kauer M, Zhang W, Lochenie C, Jee B, Albada B, Metzler-Nolte N, Pöppl A, Weber B, Muhler M, Wang Y, Schmid R, Fischer RA (2014) Structural complexity in metal–orrganic frameworks: simultaneous modification of open metal sites and hierarchical porosity by systematic doping with defective linkers. J Am Chem Soc 136:9627–9636

25. Li W, Henke S, Cheetham AK (2014) Research update: mechanical properties of metal–organic frameworks—influence of structure and chemical bonding. APL Mater 2:123902

26. Jeong W, Lim D-W, Kim S, Harale A, Yoon M, Suh MP, Kim J (2017) Modeling adsorption properties of structurally deformed metal–organic frameworks using structure–property map. Proc Natl Acad Sci USA 114:7923–7928

27. Jiang H-L, Makal TA, Zhou H-C (2013) Interpenetration control in metal–organic frameworks for functional applications. Coord Chem Rev 257:2232–2249

28. Haldar R, Sikdar N, Maji TK (2015) Interpenetration in coordination polymers: structural diversities toward porous functional materials. Mater Today 18:97–116

29. Networks, topologies, and entanglements. In: Making crystals by design, pp 58–85. https://doi.org/10.1002/9783527610112.ch3

30. Topology. In: Introduction to reticular chemistry, pp 429–452. https://doi.org/10.1002/9783527821099.ch18

31. Gong Y-N, Zhong D-C, Lu T-B (2016) Interpenetrating metal–organic frameworks. CrystEngComm 18:2596–2606

32. Öhrström L (2015) Let's talk about MOFs—topology and terminology of metal–orrganic frameworks and why we need them. Crystals 5:154–162

33. Frank M, Johnstone MD, Clever GH (2016) interpenetrated cage structures. Chemistry 22:14104–14125

34. Zhu R, Ding J, Jin L, Pang H (2019) Interpenetrated structures appeared in supramolecular cages, MOFs, COFs. Coord Chem Rev 389:119–140

35. Yaghi OM (2007) A tale of two entanglements. Nat Mater 6:92

36. Zhao D, Timmons DJ, Yuan D, Zhou H-C (2011) Tuning the topology and functionality of metal–organic frameworks by ligand design. Acc Chem Res 44:123–133

37. Batten SR, Robson R (1998) Interpenetrating nets: ordered, periodic entanglement. Angew Chem Int Ed 37:1460–1494

38. Batten SR (2001) Topology of interpenetration. CrystEngComm 3:67–72

39. Li N, Xu J, Feng R, Hu T-L, Bu X-H (2016) Governing metal–organic frameworks towards high stability. Chem Commun 52:8501–8513

40. Yin Z, Zhou Y-L, Zeng M-H, Kurmoo M (2015) The concept of mixed organic ligands in metal–orrganic frameworks: design, tuning and functions. Dalton Trans 44:5258–5275

41. Cairns AB, Goodwin AL (2013) Structural disorder in molecular framework materials. Chem Soc Rev 42:4881–4893

42. Farha OK, Hupp JT (2010) Rational design, synthesis, purification, and activation of metal–organic framework materials. Acc Chem Res 43:1166–1175

43. Liu J, Thallapally PK, McGrail BP, Brown DR, Liu J (2012) Progress in adsorption-based CO_2 capture by metal–organic frameworks. Chem Soc Rev 41:2308–2322

44. Li H, Wang K, Sun Y, Lollar CT, Li J, Zhou H-C (2018) Recent advances in gas storage and separation using metal–organic frameworks. Mater Today 21:108–121

45. Morris RE, Brammer L (2017) Coordination change, lability and hemilability in metal–organic frameworks. Chem Soc Rev 46:5444–5462

46. Liang W, Bhatt PM, Shkurenko A, Adil K, Mouchaham G, Aggarwal H, Mallick A, Jamal A, Belmabkhout Y, Eddaoudi M (2019) A tailor-made interpenetrated MOF with exceptional carbon-capture performance from flue gas. Chem 5:950–963

47. Ma S, Sun D, Ambrogio M, Fillinger JA, Parkin S, Zhou H-C (2007) Framework-catenation isomerism in metal–organic frameworks and its impact on hydrogen uptake. J Am Chem Soc 129:1858–1859

48. Burtch NC, Walton KS (2015) Modulating adsorption and stability properties in pillared metal–orrganic frameworks: a model system for understanding ligand effects. Acc Chem Res 48:2850–2857

49. Carlucci L, Ciani G, Proserpio DM, Mitina TG, Blatov VA (2014) Entangled two-dimensional coordination networks: a general survey. Chem Rev 114:7557–7580

50. Kwon O, Park S, Zhou H-C, Kim J (2017) Computational prediction of hetero-interpenetration in metal–organic frameworks. Chem Commun 53:1953–1956

51. Babarao R, Coghlan CJ, Rankine D, Bloch WM, Gransbury GK, Sato H, Kitagawa S, Sumby CJ, Hill MR, Doonan CJ (2014) Does functionalisation enhance CO_2 uptake in interpenetrated MOFs? An examination of the IRMOF-9 series. Chem Commun 50:3238–3241

52. Bara D, Wilson C, Mörtel M, Khusniyarov MM, Ling S, Slater B, Sproules S, Forgan RS (2019) Kinetic control of interpenetration in Fe–biphenyl-4,4′-dicarboxylate metal–orrganic frameworks by coordination and oxidation modulation. J Am Chem Soc 141:8346–8357

53. Vicent-Morales M, Vitorica-Yrezabal IJ, Souto M, Minguez Espallargas G (2019) Influence of interpenetration on the flexibility of MUV-2. CrystEngComm 21:3031–3035

54. Dan-Hardi M, Chevreau H, Devic T, Horcajada P, Maurin G, Férey G, Popov D, Riekel C, Wuttke S, Lavalley J-C, Vimont A, Boudewijns T, de Vos D, Serre C (2012) How interpenetration ensures rigidity and permanent porosity in a highly flexible hybrid solid. Chem Mater 24:2486–2492

55. Dincă M, Dailly A, Tsay C, Long JR (2008) Expanded sodalite-type metal–organic frameworks: increased stability and H_2 adsorption through ligand-directed catenation. Inorg Chem 47:11–13

56. Ye Y, Xiong S, Wu X, Zhang L, Li Z, Wang L, Ma X, Chen Q-H, Zhang Z, Xiang S (2016) Microporous metal–orrganic framework stabilized by balanced multiple host-couteranion hydrogen-bonding interactions for high-density CO_2 capture at ambient conditions. Inorg Chem 55:292–299

57. Jiang M, Li B, Cui X, Yang Q, Bao Z, Yang Y, Wu H, Zhou W, Chen B, Xing H (2018) Controlling pore shape and size of interpenetrated anion-pillared ultramicroporous materials enables molecular sieving of CO_2 combined with ultrahigh uptake capacity. ACS Appl Mater Interfaces 10:16628–16635

58. Lahoz-Martín FD, Calero S, Gutiérrez-Sevillano JJ, Martin-Calvo A (2017) Adsorptive separation of ethane and ethylene using isoreticular metal–orrganic frameworks. Microporous Mesoporous Mater 248:40–45

59. Yang Q-Y, Lama P, Sen S, Lusi M, Chen K-J, Gao W-Y, Shivanna M, Pham T, Hosono N, Kusaka S, Perry Iv JJ, Ma S, Space B, Barbour LJ, Kitagawa S, Zaworotko MJ (2018) Reversible switching between highly porous and nonporous phases of an interpenetrated diamondoid coordination network that exhibits gate-opening at methane storage pressures. Angew Chem Int Ed 57:5684–5689

60. Lapidus SH, Halder GJ, Chupas PJ, Chapman KW (2013) Exploiting high pressures to generate porosity, polymorphism, and lattice expansion in the nonporous molecular framework Zn(CN)2. J Am Chem Soc 135:7621–7628

61. Aggarwal H, Das RK, Bhatt PM, Barbour LJ (2015) Isolation of a structural intermediate during switching of degree of interpenetration in a metal–organic framework. Chem Sci 6:4986–4992

62. Zhang J, Wojtas L, Larsen RW, Eddaoudi M, Zaworotko MJ (2009) Temperature and concentration control over interpenetration in a metal–organic material. J Am Chem Soc 131:17040–17041

63. Wang Y, Cheng L, Wang KJ, Perry Z, Jia W, Chen R, Wang ZL, Pang JD (2019) Temperature-controlled degree of interpenetration in a single-crystal-to-single-crystal transformation within two Co(II)-triazole frameworks. Inorg Chem 58:18–21

64. Elsaidi SK, Mohamed MH, Wojtas L, Chanthapally A, Pham T, Space B, Vittal JJ, Zaworotko MJ (2014) Putting the squeeze on CH_4 and CO_2 through control over interpenetration in diamondoid nets. J Am Chem Soc 136:5072–5077

65. Ferguson A, Liu L, Tapperwijn SJ, Perl D, Coudert F-X, Van Cleuvenbergen S, Verbiest T, van der Veen MA, Telfer SG (2016) Controlled partial interpenetration in metal–organic frameworks. Nat Chem 8:250

66. Rankine D, Avellaneda A, Hill MR, Doonan CJ, Sumby CJ (2012) Control of framework interpenetration for in situ modified hydroxyl functionalised IRMOFs. Chem Commun 48:10328–10330

67. Prasad TK, Suh MP (2012) Control of interpenetration and gas-sorption properties of metal–organic frameworks by a simple change in ligand design. Chem A Eur J 18:8673–8680

68. Lun DJ, Waterhouse GIN, Telfer SG (2011) A general thermolabile protecting group strategy for organocatalytic metal–organic frameworks. J Am Chem Soc 133:5806–5809

69. Feng D, Wang K, Wei Z, Chen Y-P, Simon CM, Arvapally RK, Martin RL, Bosch M, Liu T-F, Fordham S, Yuan D, Omary MA, Haranczyk M, Smit B, Zhou H-C (2014) Kinetically tuned dimensional augmentation as a versatile synthetic route towards robust metal–organic frameworks. Nat Commun 5:5723

70. Lippke J, Brosent B, von Zons T, Virmani E, Lilienthal S, Preuße T, Hülsmann M, Schneider AM, Wuttke S, Behrens P, Godt A (2017) Expanding the group of porous interpenetrated Zr-organic frameworks (PIZOFs) with linkers of different lengths. Inorg Chem 56:748–761

71. Lu JY, Fernandez WA, Ge Z, Abboud KA (2005) A novel two-fold interpenetrating 3D 42.84 network self-assembled from a new 1D coordination polymer. New J Chem 29:434–438

72. Park J, Hong S, Moon D, Park M, Lee K, Kang S, Zou Y, John RP, Kim GH, Lah MS (2007) Porous metal–orrganic frameworks based on metal–orrganic polyhedra with nanosized cavities as supramolecular building blocks: two-fold interpenetrating primitive cubic networks of [Cu6L8]12 + nanocages. Inorg Chem 46:10208–10213

73. Volkringer C, Loiseau T, Marrot J, Ferey G (2009) A MOF-type magnesium benzene-1,3,5-tribenzoate with two-fold interpenetrated ReO_3 nets. CrystEngComm 11:58–60

74. Su Z, Fan J, Sun W-Y (2013) Novel two-fold interpenetrated metal–orrganic framework with triple-stranded right- and left-handed helical chains. Inorg Chem Commun 27:18–21

75. Li F, Hong Y-S, Zuo K-X, Sun Q, Gao E-Q (2019) Highly selective fluorescent probe for Hg^{2+} and MnO^{4-} by the two-fold interpenetrating metal–organic framework with nitro functionalized linkers. J Solid State Chem 270:509–515

76. Mir MH, Kitagawa S, Vittal JJ (2008) Two- and three-fold interpenetrated metal–organic frameworks from one-pot crystallization. Inorg Chem 47:7728–7733

77. Wang X, Lin H, Mu B, Tian A, Liu G (2010) Encapsulation of discrete $(H_2O)12$ clusters in a 3D three-fold interpenetrating metal–organic framework host with (3,4)-connected topology. Dalton Trans 39:6187–6189

78. Hu J-S, Zhu C-L, Song X-M, He J (2012) A three-folded interpenetrated metal–organic framework constructed by H-bonding interaction. Mendeleev Commun 22:220–221

79. Santra A, Lah MS, Bharadwaj PK (2014) A partially fluorinated three-fold interpenetrated stable metal–organic framework with selective CO_2 uptake. Z Anorg Allg Chem 640:1134–1140

80. Huang S-y, Li J-q, Wu X-l, Zhang X-m, Luo M-b, Luo F (2014) A novel 4-connected binodal Moganite net with three-fold interpenetration. Inorg Chem Commun 39:1–4

81. Yang E, Ding Q, Kang Y, Wang F (2014) A photoluminescent metal–organic framework with threefold interpenetrated diamond topological net. J Mol Struct 1072:228–231

82. Tynan E, Jensen P, Kelly NR, Kruger PE, Lees AC, Moubaraki B, Murray KS (2004) The ligand, the metal and the Holey'-host: synthesis, structural and magnetic characterization of Co(II), Ni(II) and Mn(II) metal–organic frameworks incorporating 4,4′-dicarboxy-2,2′-bipyridine. Dalton Trans 2004:3440–3447

83. Xu J, Bai Z-s, Chen M-s, Su Z, Chen S-s, Sun W-y (2009) Metal–organic frameworks with six- and four-fold interpenetration and their photoluminescence and adsorption property. CrystEngComm 11:2728–2733

84. Wu J, Liu J-Q, Jia Z-B, Li Q-L, Li K-B, Li H, Daiguebonne C, Calvez G, Guillou O (2014) A new 3D four-fold interpenetrated dia-like polymer: gas sorption and computational analyses. CrystEngComm 16:10410–10417

85. Zhu H-B, Shen Y, Fu Z-Z, Yu Y-Y, Jiang Y-F, Zhao Y (2019) A multifunctional Zn(II)-based four-fold interpenetrated metal–organic framework for highly sensitive sensing 2,4,6-trinitrophenol (TNP), nitrofurazone (NFZ) and nitrofurantoin (NFT). Inorg Chem Commun 103:21–24

86. Chen Y-Q, Li G-R, Chang Z, Qu Y-K, Zhang Y-H, Bu X-H (2013) A Cu(i) metal–organic framework with 4-fold helical channels for sensing anions. Chem Sci 4:3678–3682

87. Wen G-L, Wang Y-Y, Zhang Y-N, Yang G-P, Fu A-Y, Shi Q-Z (2009) A novel polythreaded metal–organic framework with inherent features of different side arms and five-fold interpenetration. CrystEngComm 11:1519–1521

88. Wei Y-L, Li J-B, Song W-C, Zang S-Q (2012) Five-fold interpenetrating diamondlike 3D metal–organic frameworks constructed from the rigid 1,2-di(pyridin-4-yl)ethane-1,2-diol ligand and aromatic carboxylate. Inorg Chem Commun 15:16–20

89. Liu C, Cui G-H, Zou K-Y, Zhao J-L, Gou X-F, Li Z-X (2013) Unusual six-connected self-catenated network with 5-fold interpenetrated CdSO4 subnets: stepwise synthesis, topology analysis and fluorescence properties. CrystEngComm 15:324–331

90. Huo J, Yan S, Li H, Yu D, Arulsamy N (2018) Three new 5-fold interpenetrating diamondoid frameworks constructed by rigid diimidazole and dicarboxylate ligands. J Mol Struct 1156:224–229

91. Lu Y-M, Lan Y-Q, Xu Y-H, Su Z-M, Li S-L, Zang H-Y, Xu G-J (2009) Interpenetrating metal–organic frameworks formed by self-assembly of tetrahedral and octahedral building blocks. J Solid State Chem 182:3105–3112

92. Wu Q-R, Wang J-J, Hu H-M, Wang B-C, Wu X-L, Fu F, Li D-S, Yang M-L, Xue G-L (2010) Two novel cadmium(II) coordination polymers based on bis-functionalized ligand 4′-(4-carboxyphenyl)-2,2′:6′,2″-terpyridine. Inorg Chem Commun 13:715–719

93. Wang N, Ma J-G, Shi W, Cheng P (2012) Two novel Cd(II) complexes with unprecedented four- and six-fold interpenetration. CrystEngComm 14:5198–5202

94. Xu H, Bao W, Xu Y, Liu X, Shen X, Zhu D (2012) An unprecedented 3D/3D hetero-interpenetrated MOF built from two different nodes, chemical composition, and topology of networks. CrystEngComm 14:5720–5722

95. Zhou X, Li B, Li G, Qi Z, Shi Z, Feng S (2012) Synthesis, structures and luminescent properties of cadmium(II) metal organic frameworks based on 3-pyrid-4-ylbenzoic acid, 4-pyrid-4-ylbenzoic acid ligands. CrystEngComm 14:4664–4669

96. Kole GK, Vittal JJ (2013) Solid-state reactivity and structural transformations involving coordination polymers. Chem Soc Rev 42:1755–1775

97. Luo Q-D, Fan C-B, Zhang X, Meng X-M, Zhu Z, Jin F, Fan Y-H (2017) 5- and 7-fold interpenetrating 3D NiII/CoII MOFs modulated by dicarboxylate and bis(imidazole) mixed ligands: syntheses, topology structure, photodegradation properties. Inorg Chem Commun 76:108–113

98. Mei L, Wang C-z, Zhu L-z, Gao Z-q, Chai Z-f, Gibson JK, Shi W-q (2017) Exploring new assembly modes of uranyl terephthalate: templated syntheses and structural regulation of a series of rare 2D → 3D polycatenated frameworks. Inorg Chem 56:7694–7706

99. Lysenko AB, Govor EV, Krautscheid H, Domasevitch KV (2006) Metal–organic frameworks incorporating Cu3(μ3-OH) clusters. Dalton Trans 2006:3772–3776

100. Rivera-Carrillo M, Chakraborty I, Raptis RG (2010) Systematic synthesis of a metal organic framework based on triangular Cu3(μ3-OH) secondary building units: from a 0-D complex to a 1-D chain and a 3-D lattice. Cryst Growth Des 10:2606–2612

101. Cheng X-C, Zhu X-H, Kuai H-W (2012) Eight-fold interpenetrating diamond-like metal–organic frameworks constructed with an N- and O-donor ligand for cadmium(II) and manganese(II). Z Naturforsch B J Chem Sci 67:1248–1254

102. Sun D, Yan Z-H, Liu M, Xie H, Yuan S, Lu H, Feng S, Sun D (2012) Three- and eight-fold interpenetrated ThSi2 metal–organic frameworks fine-tuned by the length of ligand. Cryst Growth Des 12:2902–2907

103. Huang S-y, Li J-q, Wu X-l, Zhang X-m, Luo M-b, Luo F (2014) A new acrylamide MOF with sra net showing an uncommon eight-fold interpenetration. Inorg Chem Commun 44:29–31

104. Zhou M, Yan D, Dong Y, He X, Xu Y (2017) Chiral [Mo8O26]4-polyoxoanion-induced three-dimensional architectures with homochiral eight-fold interpenetrated metal–organic frameworks. Inorg Chem 56:9036–9043

105. Dang L-l, Li J-q, Liu S-j, Luo M-b, Luo F (2014) A new acylamide MOF showing uncommon ten-fold interpenetration. Inorg Chem Commun 45:30–32

106. Ahmad M, Katoch R, Garg A, Bharadwaj PK (2014) A novel 3D 10-fold interpenetrated homochiral coordination polymer: large spontaneous polarization, dielectric loss and emission studies. CrystEngComm 16:4766–4773

107. Yaghi OM, Li H (1995) Hydrothermal synthesis of a metal–organic framework containing large rectangular channels. J Am Chem Soc 117:10401–10402
108. Chen B, Eddaoudi M, Hyde ST, O'Keeffe M, Yaghi OM (2001) Interwoven metal–organic framework on a periodic minimal surface with extra-large pores. Science 291:1021–1023
109. Sun D, Ma S, Ke Y, Collins DJ, Zhou H-C (2006) An interweaving MOF with high hydrogen uptake. J Am Chem Soc 128:3896–3897
110. Rowsell JLC, Yaghi OM (2006) Effects of functionalization, catenation, and variation of the metal oxide and organic linking units on the low-pressure hydrogen adsorption properties of metal–organic frameworks. J Am Chem Soc 128:1304–1315
111. Maji TK, Matsuda R, Kitagawa S (2007) A flexible interpenetrating coordination framework with a bimodal porous functionality. Nat Mater 6:142–148
112. Ma S, Wang X-S, Yuan D, Zhou H-C (2008) A coordinatively linked Yb metal–organic framework demonstrates high thermal stability and uncommon gas-adsorption selectivity. Angew Chem Int Ed 47:4130–4133
113. Hafizovic J, Bjørgen M, Olsbye U, Dietzel PDC, Bordiga S, Prestipino C, Lamberti C, Lillerud KP (2007) The inconsistency in adsorption properties and powder XRD data of MOF-5 Is rationalized by framework interpenetration and the presence of organic and inorganic species in the nanocavities. J Am Chem Soc 129:3612–3620
114. Liu L, Yao Z, Ye Y, Lin Q, Chen S, Zhang Z, Xiang S (2018) Enhanced intrinsic proton conductivity of metal–organic frameworks by tuning the degree of interpenetration. Cryst Growth Des 18:3724–3728
115. Gupta V, Mandal SK (2019) A robust and water-stable two-fold interpenetrated metal–organic framework containing both rigid tetrapodal carboxylate and rigid bifunctional nitrogen linkers exhibiting selective CO_2 capture. Dalton Trans 48:415–425
116. Shi Z-Q, Guo Z-J, Zheng H-G (2015) Two luminescent Zn(ii) metal–organic frameworks for exceptionally selective detection of picric acid explosives. Chem Commun 51:8300–8303
117. Tan A-d, Wang Y-f, Fu Z-y, Tsiakaras P, Liang Z-x (2017) Highly effective oxygen reduction reaction electrocatalysis: Nitrogen-doped hierarchically mesoporous carbon derived from interpenetrated nonporous metal–organic frameworks. Appl Catal B 218:260–266
118. Liu Y-L, Yue K-F, Shan B-H, Xu L-L, Wang C-J, Wang Y-Y (2012) A new 3-fold interpenetrated metal–organic framework (MOF) based on trinuclear zinc(II) clusters as secondary building unit (SBU). Inorg Chem Commun 17:30–33
119. Wu H-Y, Wang R-X, Yang W, Chen J, Sun Z-M, Li J, Zhang H (2012) 3-fold-interpenetrated uranium-organic frameworks: new strategy for rationally constructing three-dimensional uranyl organic materials. Inorg Chem 51:3103–3107
120. Mei L, Wu Q-y, An S-w, Gao Z-q, Chai Z-f, Shi W-q (2015) Silver ion-mediated heterometallic three-fold interpenetrating uranyl-organic framework. Inorg Chem 54:10934–10945
121. Zhang Y, Wang L, Yao R-X, Zhang X-M (2017) Fourfold-interpenetrated MOF [Ni(pybz)2] as coating material in gas chromatographic capillary column for separation. Inorg Chem 56:8912–8919
122. Aggarwal H, Das RK, Engel ER, Barbour LJ (2017) A five-fold interpenetrated metal–organic framework showing a large variation in thermal expansion behaviour owing to dramatic structural transformation upon dehydration–rehydration. Chem Commun 53:861–864
123. Zhang X-T, Chen H-T, Li B, Liu G-Z, Liu X-Z (2018) 3-Fold and 6-Fold interpenetrating diamond nets based on the designed N, N'-dioxide 3,3'-benzo(c)cinnoline dicarboxylic acid with highly sensitive luminescence sensing for NACs and Fe^{3+} ion. J Solid State Chem 267:28–34
124. Kang X-M, Cheng R-R, Xu H, Wang W-M, Zhao B (2017) A sensitive luminescent acetylacetone probe based on Zn-MOF with six-fold interpenetration. Chem A Eur J 23:13289–13293
125. Song B-Q, Qin C, Zhang Y-T, An L-T, Shao K-Z, Su Z-M (2015) A novel [4+3] interpenetrated net containing 7-fold interlocking pseudo-helical chains and exceptional catenane-like motifs. Dalton Trans 44:2844–2851
126. Li S-L, Han M, Zhang Y, Li G-P, Li M, He G, Zhang X-M (2019) X-ray and UV dual photochromism, thermochromism, electrochromism, and amine-selective chemochromism in an Anderson-like Zn7 cluster-based 7-fold interpenetrated framework. J Am Chem Soc 141:12663–12672
127. Cheng X, Zhu X-H, Kuai H-W (2012) Eight-fold interpenetrating diamond-like metal–organic frameworks constructed with an N- and O-donor ligand for cadmium(II) and Manganese(II). Chemistry 67b. https://doi.org/10.5560/znb.2012-0215

128. Chen Z, Gallo G, Sawant VA, Zhang T, Zhu M, Liang L, Chanthapally A, Bolla G, Quah HS, Liu X, Loh KP, Dinnebier RE, Xu Q-H, Vittal JJ (2019) Giant enhancement of second harmonic generation accompanied by the structural transformation of 7-fold to 8-fold interpenetrated metal–organic framework (MOF). Angew Chem Int Ed. doi: 10.1002/anie.201911632
129. Tseng T-W, Luo T-T, Tsai C-C, Lu K-L (2015) A huge diamondoid metal–organic framework with a neo-mode of tenfold interpenetration. CrystEngComm 17:2935–2939
130. Loukopoulos E, Michail A, Kostakis GE (2018) A 12-fold ThSi2 interpenetrated network utilizing a glycine-based pseudopeptidic ligand. Crystals 8:47
131. Wu H, Yang J, Su Z-M, Batten SR, Ma J-F (2011) An exceptional 54-fold interpenetrated coordination polymer with 103-srs network topology. J Am Chem Soc 133:11406–11409
132. Yang S, Lin X, Lewis W, Suyetin M, Bichoutskaia E, Parker JE, Tang CC, Allan DR, Rizkallah PJ, Hubberstey P, Champness NR, Mark Thomas K, Blake AJ, Schröder M (2012) A partially interpenetrated metal–organic framework for selective hysteretic sorption of carbon dioxide. Nat Mater 11:710
133. Verma G, Kumar S, Pham T, Niu Z, Wojtas L, Perman JA, Chen Y-S, Ma S (2017) Partially interpenetrated NbO topology metal–organic framework exhibiting selective gas adsorption. Cryst Growth Des 17:2711–2717
134. O'Nolan D, Madden DG, Kumar A, Chen K-J, Pham T, Forrest KA, Patyk-Kazmierczak E, Yang Q-Y, Murray CA, Tang CC, Space B, Zaworotko MJ (2018) Impact of partial interpenetration in a hybrid ultramicroporous material on C_2H_2/C_2H_4 separation performance. Chem Commun 54:3488–3491
135. https://wcs.webofknowledge.com/RA/analyze.do?product=UA&SID=7A4qH71EpekB6LeZp8t&field=PY_PublicationYear_PublicationYear_en&yearSort=true

Ⓐ Springer